NASA CR-134659

DESIGN, CONSTRUCTION AND EVALUATION OF A 12.2 GHz, 4.0 KW-CW HIGH EFFICIENCY KLYSTRON AMPLIFIER

by J. M. Nishida and L. K. Brodersen

VARIAN ASSOCIATES

prepared for

NATIONAL AERONAUTICS AND SPACE ADMINISTRATION

NASA Lewis Research Center
Contract NAS3-13726

1. Report No. NASA CR-134659	2. Government Accession No.	3. Recipient's Catalog No.
4. Title and Subtitle DESIGN, CONSTRUCTION AND EVALUATION OF A 12.2 GHz, 4.0 kW-CW HIGH EFFICIENCY KLYSTRON AMPLIFIER		5. Report Date AUGUST 1974
		6. Performing Organization Code
7. Author(s) J. M. Nishida and L. K. Bordersen		8. Performing Organization Report No.
		10. Work Unit No.
9. Performing Organization Name and Address Varian Associates Palo Alto Tube Division 611 Hansen Way Palo Alto, California 94303		11. Contract or Grant No. NAS 3-13276
		13. Type of Report and Period Covered Final Report
12. Sponsoring Agency Name and Address National Aeronautics and Space Administration Washington, D. C. 20546		14. Sponsoring Agency Code

15. Supplementary Notes

Project Manager, P. Ramins, NASA Lewis Research Center, Cleveland, Ohio.

16. Abstract

This report describes an analytical and experimental program to study design techniques for optimizing the conversion efficiency of klystron amplifiers, and to utilize these techniques in the development and fabrication of an X-band 4 kW cw klystron, intended for use in satellite-borne television broadcast transmitters.

The design is based on a technique for increasing the rf beam current by using the second harmonic space-charge forces in the bunched beam. Experimental analysis was also made of a method to enhance circuit efficiency in the klystron cavities.

The design incorporates a collector which is demountable from the tube to facilitate multistage depressed collector experiments employing a NASA-designed axisymmetric, electrostatic collector for linear beam microwave tubes.

17. Key Words (Suggested by Author(s)) Conversion efficiency of klystron amplifiers Satellite-borne television broadcast transmitters Second harmonic space-charge forces Demountable collector Multistage Depressed Collector	18. Distribution Statement Unclassified - Unlimited

19. Security Classif. (of this report) Unclassified	20. Security Classif. (of this page) Unclassified	21. No. of Pages 74	22. Price* $3.00

FOREWORD

The work described herein was done by Varian Associates, Palo Alto Tube Division under NASA Contract NAS3-13726 with Mr. J. M. Nishida as principal investigator. Others working on the project included Mr. E. L. Lien, Mr. G. V. Miram and Mr. A. E. Berwick. Mr. P. Ramins, NASA-Lewis Research Center, was Project Manager.

Preceding page blank

iii

ABSTRACT

This report describes an analytical and experimental program to study design techniques for optimizing the conversion efficiency of klystron amplifiers, and to utilize these techqniues in the development and fabrication of an X-band 4 kW cw klystron, intended for use in satellite-borne television broadcast transmitters.

The design is based on a technique for increasing the rf beam current by using the second harmonic space-charge forces in the bunched beam. Experimental analysis was also made of a method to enhance circuit efficiency in the klystron cavities.

The design incorporates a collector which is demountable from the tube to facilitate multi-stage depressed collector experiments employing a NASA-designed axisymmetric, electrostatic collector for linear beam microwave tubes.

TABLE OF CONTENTS

PRECEDING PAGE BLANK NOT FILMED

LIST OF ILLUSTRATIONS

LIST OF ILLUSTRATIONS (Cont.)

LIST OF TABLES

DESIGN, CONSTRUCTION AND EVALUATION OF A 12.2 GHz, 4.0 kW CW HIGH EFFICIENCY KLYSTRON AMPLIFIER

By: J. M. Nishida and L. K. Brodersen
Varian Associates
Palo Alto, California

1.0 SUMMARY

A theoretical design for a high efficiency klystron is described. The objective was to obtain 4 kW cw with 40 MHz bandwidth at 12.2 GHz and with 50% conversion efficiency.

Both large and small signal computer programs were employed to analyze the design and to select design parameters for maximum conversion efficiency. A previously developed approach was employed, utilizing the second harmonic space-charge forces in the bunched beam to increase efficiency.

A total of three klystrons were fabricated to verify the analytical design.

The first experimental tube (SN 1) had an output cavity of toroidal configuration, designed to maximize output circuit efficiency. The conversion efficiency achieved was greater than 50%, with a measured output circuit efficiency of 95.5%. Full power cw test data could not be taken on this tube because of the high degree of thermal detuning, which tended to distort the frequency bandpass and reduce the effective output power. This problem was traced to dimensional changes in the toroidal output cavity drift tube tips, aggravated by inadequate cooling of the penultimate drift tube region.

The design of the second experimental tube (SN2) was modified to correct the difficulties observed on the first tube. The output cavity design was changed to a more conventional milled cavity type, with heavier walled drift tube tips. The drift length between the penultimate cavity and output cavity was increased to allow the addition of a water cooling passage. These changes greatly decreased the frequency drift problem, permitting operation at the full design power output. Conversion efficiency was 49.3% and the output cavity circuit efficiency was 95.4%, both values only slightly lower than those seen on the first tube.

1

The third tube (SN 3) was identical to the second, and test performance was essentially the same.

Most of the basic performance requirements were achieved. Gain and bandwidth characteristics were entirely adequate, and the conversion efficiency was very close to the goal of 50%. It was also demonstrated that a well-designed conventional output cavity could operate at approximately the same circuit efficiency as one of toroidal configuration, at least at the higher frequencies relevant to this study.

2

2.0 INTRODUCTION

This report describes a development and experimental program for a high efficiency klystron for use in a satellite television transmitter. The primary objective of this program was to demonstrate the feasibility of obtaining high interaction efficiency in a relatively narrowband klystron operating at 4 kW cw and at 12.2 GHz. Two tubes and ten demountable guns were to be delivered to Lewis Research Center. These tubes were to be operated in a space chamber and used for operation with a NASA-designed multistage depressed collector (Ref. 1,2). In addition to delivery of the hardware items, it was intended to experimentally verify analytical design techniques for circuit efficiency enhancement in klystron cavity resonators, as described in the results of Contract NAS3-11533 (Ref. 3).

The first task on the program was the development and analytic optimization of the design. This was followed by the physical design to achieve the characteristics selected. A total of three klystrons were constructed and tested. The first tube provided extensive information that was used to modify the design of the final two tubes, to better meet the performance objectives, or to eliminate experimentally observed defects.

Computed small signal gain was lower than the experimentally measured gain. Predicted efficiency was somewhat optimistic compared with experimental measurements, although final results were very close to the original design goal.

3.0 DESIGN APPROACH AND TRADE-OFF CONSIDERATIONS

The basic design approach selected was to use a conventional five cavity klystron rf circuit with drift lengths chosen to maximize conversion efficiency, using the design techniques proposed by Lien (Ref. 4). The factors which influenced the initial choice of parameters are outlined in this section.

3.1 Summary of Specifications

The major klystron specifications are summarized in Table 3.1. Those specifications which most directly affect the choice of design parameters are frequency, gain, power and efficiency. Frequency and power, taken together, place limits on the mechanical design due to thermal considerations; the choice of cavity design for high efficiency, as will be shown, may often be in conflict with these thermal considerations.

TABLE 3.1
MAJOR KLYSTRON SPECIFICATIONS

Electronic Conversion Efficiency	50% min
Frequency	12.2 GHz
Bandwidth (3 dB)	40 MHz
Power	4.0 kW min.
Gain	40 ± 1.5 dB
Design Life	2 yr. min.
Phase Linearity ($d^2\phi/d\omega^2$)	$0.005°/MHz^2$
Gain Linearity (deviation)	0.5 dB max.
Collector Magnetic Leakage	0.5% max.
Dc Beam Transmission	99.5% min.
Beam Transmission at Saturation	98% min.
Maximum Beam Voltage	16 kV
Tube and Focusing Magnet must be capable of operating inside vacuum chamber, and must be bakeable to $250°C$	
Demountable Collector	
Demountable Electron Gun	

3.2 Initial Electrical Design

The selected beam power was 8 kW, based on 50% conversion efficiency and an output power of 4 kW.

The choice of beam voltage, within the specified 16 kV maximum, was controlled by the requirement for high efficiency and the need for thermal stability weighed against the requirement for long life. Life considerations dictate limits on cathode current density. To obtain long life, the cathode current density must be kept low. To obtain good beam optics, the beam convergence must also be kept to a minimum. A low beam perveance is also desirable for high efficiency, although the length of the rf circuit increases with decreasing perveance.

The normalized tunnel diameter predominantly affects the efficiency and the beam and gun designs. The minimum practical drift tube diameter is determined by the beam size, and since the cavity R/Q is influenced by drift tube size, it is doubly important to minimize the diameter of both the beam and drift tube. Conversely, a lower limit on beam size is set by space charge effects and by beam optics and focusing considerations. The required area convergence of the gun and the magnetic focusing field decrease with increasing tunnel diameter, while the conversion efficiency decreases rapidly when the normalized tunnel radius γa exceeds 0.7 radians.

The chosen area convergence of the beam must also be large enough to assure tolerable loading of the cathode, yet small enough to provide reasonable gun optics. Experience has shown that area convergences as high as 60:1 are reasonable in the theoretical design of a gun, capable of producing a beam with excellent laminarity at low perveance. The major problem in low perveance guns stems from the fact that the location of the focus electrode relative to the cathode is more critical than in higher perveance designs. High area convergence generally complicates magnetic design in a convergent confined flow system, since it is necessary to find a magnetic flux pattern that duplicates the trajectories of the electrons in the cathode-anode region.

At lower area convergence ratios, cathode current density becomes a problem. The use of impregnated tungsten cathodes will allow long life expectation at 2 A/cm^2.

6

To provide a basis for a preliminary selection of the beam perveance and normalized tunnel diameter, the beam current density, the required magnetic focusing field, and the bandwidth of the output resonator were calculated for several combinations of these parameters. The selected ratio of beam-to-tunnel diameter was 0.65 in this calculation. The result showed that a beam perveance of 0.5 x 10^{-6} amps/volt$^{3/2}$ and a normalized tunnel radius γa of 0.75 would be a good compromise. High efficiency and the desired bandwidth could be achieved with these design parameters, and the design of the electron gun does not become too difficult. The required area convergence is 63:1, assuming a cathode loading of 2 amps/cm^2.

The remaining major design parameters are: number and Q-factor of cavities, interaction gap length, and inter-cavity drift lengths.

The selected design approach for achieving the high efficiency required was developed on a company-sponsored study program for high efficiency klystron amplifiers (Ref. 4).

An experimental tube with a conversion efficiency of 70 percent was tested during this study program. The improvement in efficiency, as compared with conventional klystrons, was obtained by increasing the rf beam current with a novel combination of second harmonic and fundamental frequency cavities in the buncher system. This design had some limitations, however, which would be undesirable for the tube to be developed on this program. The most severe restriction was that a relatively small normalized beam tunnel must be used to get sufficient coupling between the second harmonic cavity and the beam. The required magnetic focusing field and the area convergence of the electron gun would therefore have to be high.

In addition, the second harmonic cavity must be tuned relatively close to the second harmonic of the drive frequency. This would therefore limit the applicable bandwidth of the klystron. Although the use of this design approach might have been feasible, as far as bandwidth was concerned, it was decided that a slightly different approach would be used that did not have the same design restrictions.

This new design approach is functionally quite similar to the previous approach and offers approximately the same theoretical efficiency. It consists of using the second harmonic space-charge

forces in the bunched beam instead of the second harmonic circuit fields. This requires unusually long drift lengths between some of the cavities in the large-signal portion of the circuit. The overall length of the tube is therefore larger in this case. The tube could, however, be designed with a larger tunnel diameter, thus requiring a smaller area convergence for the electron gun.

The gain and phase-shift characteristics of the tube are determined by the tuning and loading of the resonators. The selected loading and tuning pattern given in Table 3.2 represents a compromise between constant gain and constant phase response. The listed values were arrived at by varying the tuning pattern and Q-factors of the buncher resonators and calculating the effect on the small-signal buncher characteristic.

Two different circuit configurations were evaluated during this analytic process. It was initially thought that a total of six cavities, resistively loaded in the buncher section, would be required to meet the specified combination of efficiency, gain, bandwidth and phase response. Subsequent calculations indicated that these specifications could be met with just 5 cavities, in a somewhat different tuning pattern and with loading removed. It was this approach that was selected, because of the reduced tube length and the elimination of the mechanical complexity and the process-control problems inherent with internal resistive loading.

In the final tuning arrangement, the output resonator is tuned to the center frequency. The frequency of resonator 4 is selected for the optimum efficiency as determined from large-signal analyses of the buncher system. The frequencies of the first three cavities are then determined by the desired small-signal gain and phase characteristics.

The selected design parameters for the tube (Table 3.2) differ only slightly from those listed in NASA CR-72461 (Ref. 5) for the 11 GHz 30 MHz bandwidth klystron design, primarily in those areas related to frequency of operation or affected by the high-efficiency design approach previously discussed. We are in close agreement with the important design parameters of beam voltage, perveance, and normalized tunnel and beam diameters.

TABLE 3.2

SUMMARY OF DESIGN PARAMETERS FOR TUBE NO. 1

Frequency	12.2 GHz
Power Output	4.0 kW min.
Efficiency	50% min.
Bandwidth (–3 dB)	40 MHz min.
Gain	40 dB min.
Beam Voltage	12.1 kV
Beam Current	0.66 amps
Beam Filling Factor, b/a	0.65
Beam Diameter, 2b	0.032 inch
Drift Tube Diameter, 2a	0.051 inch
Normalized Gap Length Buncher	1.0 radian
Output	0.7 radian
Normalized Tunnel Radius, γa	0.75 radian
Number of Cavities	5
Length of Interaction Gaps, Buncher	0.033 inch
Output	0.023 inch
Drift Lengths 1-2	0.508 inch
2-3	1.015 inch
3-4	0.761 inch
4-5	0.254 inch
Normalized Drift Length 1-2	60°
2-3	120°
3-4	90°
4-5	30°
R/Q Buncher	130
Penultimate	120
Output	85
Q_e Input	600
Q_e Output	210
Q_o Buncher	2800
Q_o Penultimate	2700
Q_o Output	3100
Output Circuit Efficiency	93.6%

4.0 ANALYTICAL DESIGN

The analytical design procedure was based on several Varian computer programs which model electron trajectories and the rf interaction process in a klystron. These programs were used to refine the initial design; i.e., to ensure that the klystron would perform with proper gain and bandwidth, as well as to predict the efficiency. Because the programs are basically analytic rather than synthetic in nature, it was necessary, in order to synthesize a design, to compute a number of designs in order to systematically optimize a given parameter.

4.1 Review of Analytic Capability

The main analytical tools used in this program were our small-signal and large-signal computer programs for klystron amplifiers, with computer programs and beam analyzers used for the electron gun and beam design.

The small-signal computer program is based on space-charge wave theory and is capable of predicting the small-signal gain and phase delay, and the first and second derivatives of the phase delay, as a function of operating frequency. The small-signal analyses were used in the selection of the number of cavities and for adjustment of the tuning and loaded Q-factors of the resonators. The final adjustment of the tuning pattern, however, was done experimentally.

The large-signal computer program used in the tube analysis is based on a program developed at Cornell University, modified to account for the effect of the drift tube on the rf space charge forces (Ref. 6). This program has been capable of predicting the efficiency of klystron amplifiers within about 5 percentage points at the 50 percent efficiency level, and within about 10 percentage points at the 70 percent efficiency level. The large-signal program is used for comparison of the efficiency of different designs and for calculation of the optimum loading of the output resonator. No specific large-signal calculations were made for this tube design, but use was made of the general design concepts for selection of parameters derived in previous company-sponsored study programs (Ref. 4).

The gun design computer program solves the electron trajectories for arbitrary beam flow problems including space charge, axially symmetric magnetic fields, relativistic effects (including the self-magnetic field of the beam) and the effects of thermal velocities. In addition to the design of electron guns, collector beam spread calculations may also be performed with this program.

Varian's beam tester thoroughly evaluates the performance of actual gun configurations. Salient features of this machine include a pinhole and split collector arrangement which can be used to scan the beam in two transverse directions as well as along the beam axis, a well shielded solenoid so that measurements can be made with an applied focusing field, and an oil-free vacuum chamber.

4.2 Small-Signal Analysis

The initial small-signal analysis began by using assumed design parameters selected as feasible values from previous work on similar tubes. This was primarily a verification process to show that the basic tube specifications could be met with a five cavity approach, and will not be discussed in detail. The next step was the actual design and cold test of the individual cavities, providing measured cavity characteristics for use in the small-signal computer calculations.

The chosen and measured parameters for the first tube are listed in Table 3.2. These figures were used to compute the small-signal gain, bandwidth and phase response. The results of the final computations for the first tube are shown in Figure 4-1, which is the actual computer terminal printout. The small-signal gain is 57.9 dB with a maximum deviation across the 40 MHz bandwidth of ±0.74 dB. The actual saturated gain is typically about 6.0 dB less than the calculated small-signal gain, resulting in a predicted saturated gain of approximately 52.0 dB. As will be seen by the actual test results for the first tube, measured gain at saturation was 61 dB. This discrepancy between calculated and measured values is probably the result of having a larger beam diameter than that used in the calculations, and therefore larger gap coupling factors. This possibility is also supported by the high body current experienced at test.

These small-signal calculations were repeated later in the program, using the measured design parameters for the last two tubes. The main differences between these two cases were in cavity

12

```
LOAD *GBW
READY

TAPE
READY

1 DATA 5,0,0,0
2 DATA 12.1,5.5E-5,12.2,600,14.64
3 DATA .8075,.8466,130,350,0
4 DATA .8075,.8466,130,850,1.05
5 DATA .8075,.8466,130,850,2.1
6 DATA .8075,.8466,120,820,1.57
7 DATA .8382,.8709,85,180,.52
8 DATA -.002,.0002,.002,30,2
9 DATA 0,-.002,.003,.0069,0
KEY
READY

1 DATA 5,0,1,0
RUN


GBW            16:34    02/03/71   WEDNESDAY    001


GAIN-BANDWIDTH CALCULATIONS
V=   12.1 KV    G=5.5000E-05   F=12.2000 GHZ    LF1=  600    W/WQ=  14.64
```

CAV	M+	M-	R/Q	Q	EQL	DF/FO
1	0.8075	0.8466	130	350	0.000	0.0000
2	0.8075	0.8466	130	850	1.050	-0.0020
3	0.8075	0.8466	130	850	2.100	0.0030
4	0.8075	0.8466	120	820	1.570	0.0069
5	0.8382	0.8709	85	180	.520	0.0000

FREQ	DB GAIN	P DEG	DP DEG	DP/DF DEG/MHZ	D2 P DEG	D2P/DF2 DEG/MHZ↑2
-0.0020	55.49	57.0	0.00	0.000	0.0000	0.0000
-0.0018	56.51	81.9	24.89	10.201	0.0000	0.0000
-0.0016	56.84	104.0	22.18	9.088	-2.7152	-0.4561
-0.0014	56.90	122.8	18.80	7.703	-3.3792	-0.5676
-0.0012	56.95	139.2	16.34	6.698	-2.4519	-0.4118
-0.0010	57.07	154.1	14.97	6.135	-1.3754	-0.2310
-0.0008	57.26	168.5	14.38	5.893	-0.5903	-0.0992
-0.0006	57.49	182.8	14.27	5.850	-0.1055	-0.0177
-0.0004	57.71	197.2	14.41	5.905	0.1340	0.0225
-0.0002	57.87	211.8	14.58	5.974	0.1699	0.0285
0.0000	57.93	226.4	14.62	5.992	0.0426	0.0072
0.0002	57.89	240.8	14.43	5.915	-0.1873	-0.0315
0.0004	57.73	254.8	13.99	5.735	-0.4396	-0.0738
0.0006	57.50	268.2	13.35	5.473	-0.6395	-0.1074
0.0008	57.23	280.8	12.61	5.168	-0.7440	-0.1250
0.0010	56.95	292.6	11.86	4.862	-0.7467	-0.1254
0.0012	56.71	303.8	11.20	4.590	-0.6625	-0.1113
0.0014	56.53	314.5	10.69	4.382	-0.5089	-0.0855
0.0016	56.46	324.9	10.40	4.262	-0.2927	-0.0492
0.0018	56.52	335.3	10.39	4.260	-0.0039	-0.0007

40 MHZ

```
TIME    3 SECS.
```

Figure 4-1. Computer Terminal Printout of Final Computations for the First Tube

tuning pattern, output cavity Q and penultimate drift length. The final design parameters are summarized in Table 4.1. The computer printout from the gain-bandwidth-phase computation is shown in Figure 4-2.

TABLE 4.1

SUMMARY OF FINAL DESIGN PARAMETERS

Frequency	12.2 GHz
Bandwidth (–3 dB minimum)	40 MHz
Beam voltage	12.0 kV
Beam current	0.66 amps
Beam perveance	0.5×10^{-6} amps/volt$^{3/2}$
Beam area convergence	63:1
Cathode loading (maximum)	2.0 amps/cm^2
Cathode diameter	0.255 inch
Number of cavities	5
(R_{sh}/Q) of the buncher cavities	130 ohms
(R_{sh}/Q) of the output cavity	120 ohms
Normalized length of the interaction gaps:	
Buncher cavities	1.0 radian
Output cavity	0.7 radian
Length of the interaction gaps:	
Buncher cavities	0.033 inch
Output cavity	0.023 inch
Normalized tunnel radius, γa	0.75 radian
Tunnel diameter, $2a$	0.051 inch
Beam filling factor, b/a	0.65
Normalized drift lengths, $\beta_q \ell$:	
$\beta_q \ell_{1,2}$	60°
$\beta_q \ell_{2,3}$	120°
$\beta_q \ell_{3,4}$	90°
$\beta_q \ell_{4,5}$	35°
Drift lengths:	
$\ell_{1,2}$	0.508 inch
$\ell_{2,3}$	1.015 inch
$\ell_{3,4}$	0.761 inch
$\ell_{4,5}$	0.295 inch

14

TABLE 4.1

SUMMARY OF FINAL DESIGN PARAMETERS (Continued)

Total Q-factor of the cavities:

Q_{input}	600
Q_2	2800
Q_3	2800
Q_4	2700
Q_{output}	130

Cavity tuning:

f_1	12.200 GHz
f_2	12.175 GHz
f_3	12.230 GHz
f_4	12.290 GHz
f_5	12.200 GHz
Magnetic focusing field (2.5 x Brillouin field)	3850 Gauss

The computed small signal gain as a function of frequency is plotted in Figure 4-3. No attempt was made to eliminate the 2.0 dB slope seen across the 40 MHz operating band, although a slight adjustment of output cavity frequency could have accomplished this. The overall calculated band-width was quite close to that measured on the final tube design. Again the calculated small-signal gain values were somewhat pessimistic as compared to actual test results.

Figure 4-4 is a plot of computed phase shift through the tube. It shows the relative change in output phase as a function of frequency.

A linear component of 5.45°/MHz has been subtracted from the total phase shift through the tube to achieve the phase deviation curve plotted in Figure 4-5. At no point in the 10 MHz AM operating band does $\Delta\phi(\omega)$ deviate more than the required 1.2° maximum.

Figure 4-6 presents $d^2\phi(\omega)/d\omega^2$ as a function of frequency. In this case the tube meets the specified 0.05°/MHz^2 only across the central portion of the band.

TGBW

GAIN-BANDWIDTH CALCULATIONS
VO=   12.0 KV   GO= 5.4770E-05 MHO   FO=12.2000 GHZ   QE1= 600   W/WO=14.64

CAV	M+	M-	R/Q	Q	BQL	F(GHZ)
1	0.7734	0.8113	130	353	0.000	12.2000
2	0.7734	0.8113	130	878	1.058	12.1750
3	0.7734	0.8113	130	878	2.114	12.2300
4	0.7734	0.8113	130	868	1.585	12.2900
5	0.8035	0.8350	85	123	.614	12.2000

| F(GHZ)	DB GAIN	PHASE DEG	DP DEG	DP/DF DEG/MHZ	D2P DEG	D2P/DF2 DEG/MHZ↑2
12.1700	48.53	19.8	0.00	0.000	0.0000	0.0000
12.1720	50.75	35.9	16.13	8.066	3.0600	0.7650
12.1740	52.57	55.1	19.19	9.596	1.5204	0.3801
12.1760	53.75	75.8	20.71	10.356	-0.8945	-0.2236
12.1780	54.28	95.6	19.82	9.908	-2.4233	-0.6058
12.1800	54.40	113.0	17.39	8.697	-2.5136	-0.6284
12.1820	54.37	127.9	14.88	7.440	-1.9075	-0.4769
12.1840	54.34	140.9	12.97	6.486	-1.2330	-0.3083
12.1860	54.38	152.6	11.74	5.870	-0.6976	-0.1744
12.1880	54.48	163.6	11.04	5.521	-0.3168	-0.0792
12.1900	54.66	174.4	10.73	5.363	-0.0635	-0.0159
12.1920	54.87	185.0	10.66	5.331	0.0860	0.0215
12.1940	55.11	195.8	10.75	5.374	0.1464	0.0366
12.1960	55.33	206.7	10.89	5.447	0.1291	0.0323
12.1980	55.53	217.7	11.02	5.512	0.0502	0.0126
12.2000	55.68	228.8	11.07	5.537	-0.0656	-0.0164
12.2020	55.77	239.8	11.01	5.504	-0.1874	-0.0468
12.2040	55.82	250.6	10.82	5.410	-0.2848	-0.0712
12.2060	55.83	261.1	10.54	5.268	-0.3367	-0.0842
12.2080	55.82	271.3	10.20	5.099	-0.3332	-0.0833
12.2100	55.82	281.2	9.87	4.933	-0.2732	-0.0683
12.2120	55.86	290.8	9.59	4.796	-0.1578	-0.0394
12.2140	55.94	300.2	9.43	4.717	0.0158	0.0039
12.2160	56.10	309.7	9.45	4.725	0.2590	0.0648
12.2180	56.35	319.4	9.71	4.855	0.5952	0.1488
12.2200	56.70	329.7	10.30	5.152	1.0575	0.2644
12.2220	57.15	341.1	11.36	5.681	1.6662	0.4166
12.2240	57.65	354.1	13.03	6.514	2.3398	0.5849
12.2260	58.11	369.5	15.37	7.684	2.6853	0.6713
12.2280	58.31	387.5	18.05	9.027	1.9160	0.4790
12.2300	57.98	407.5	19.97	9.985	0.0000	0.0000

PROCESSING   4 UNITS

Figure 4-2.   Computer Printout from the Gain-Bandwidth-Phase
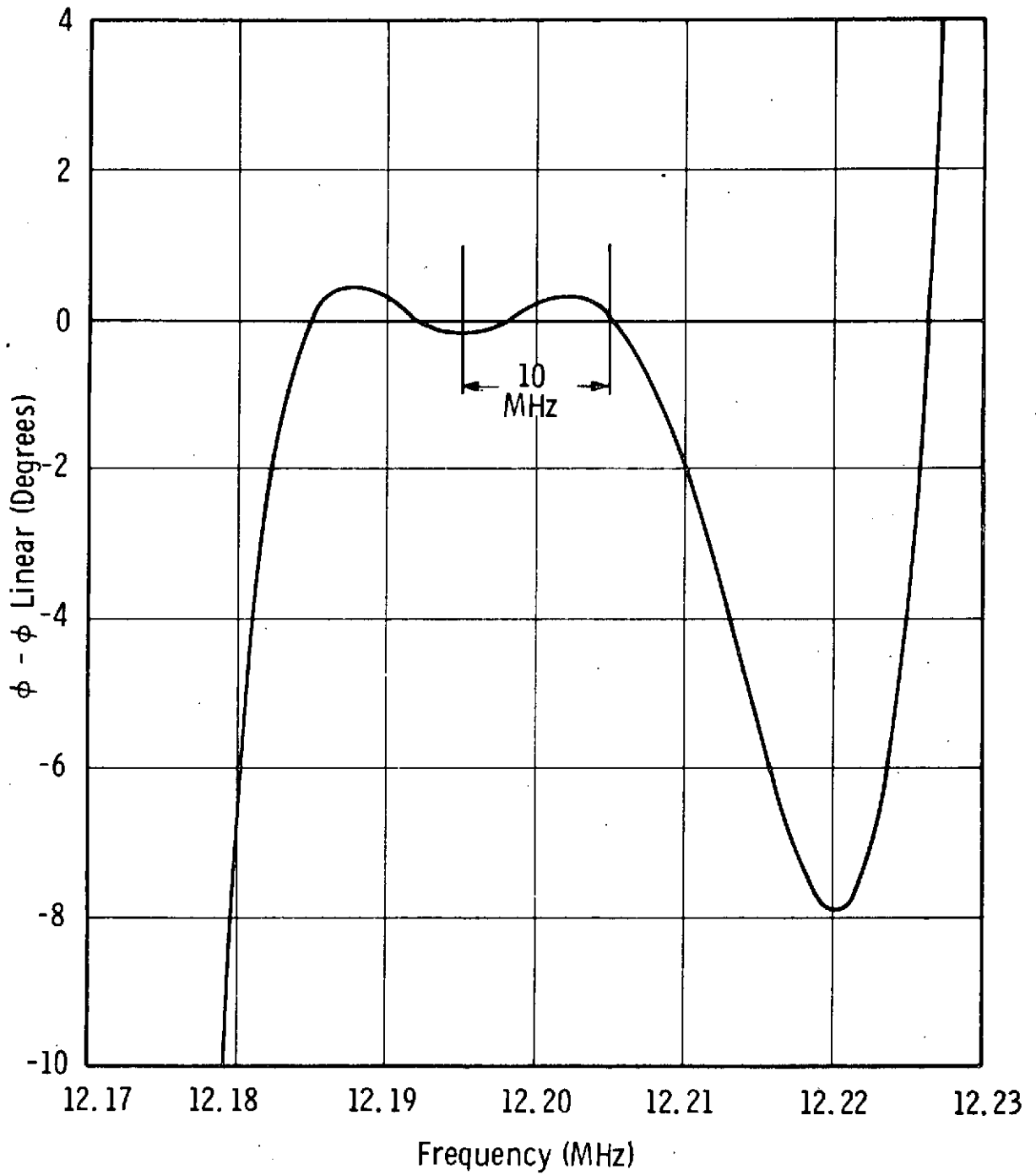Computation for Final Cavity Configuration
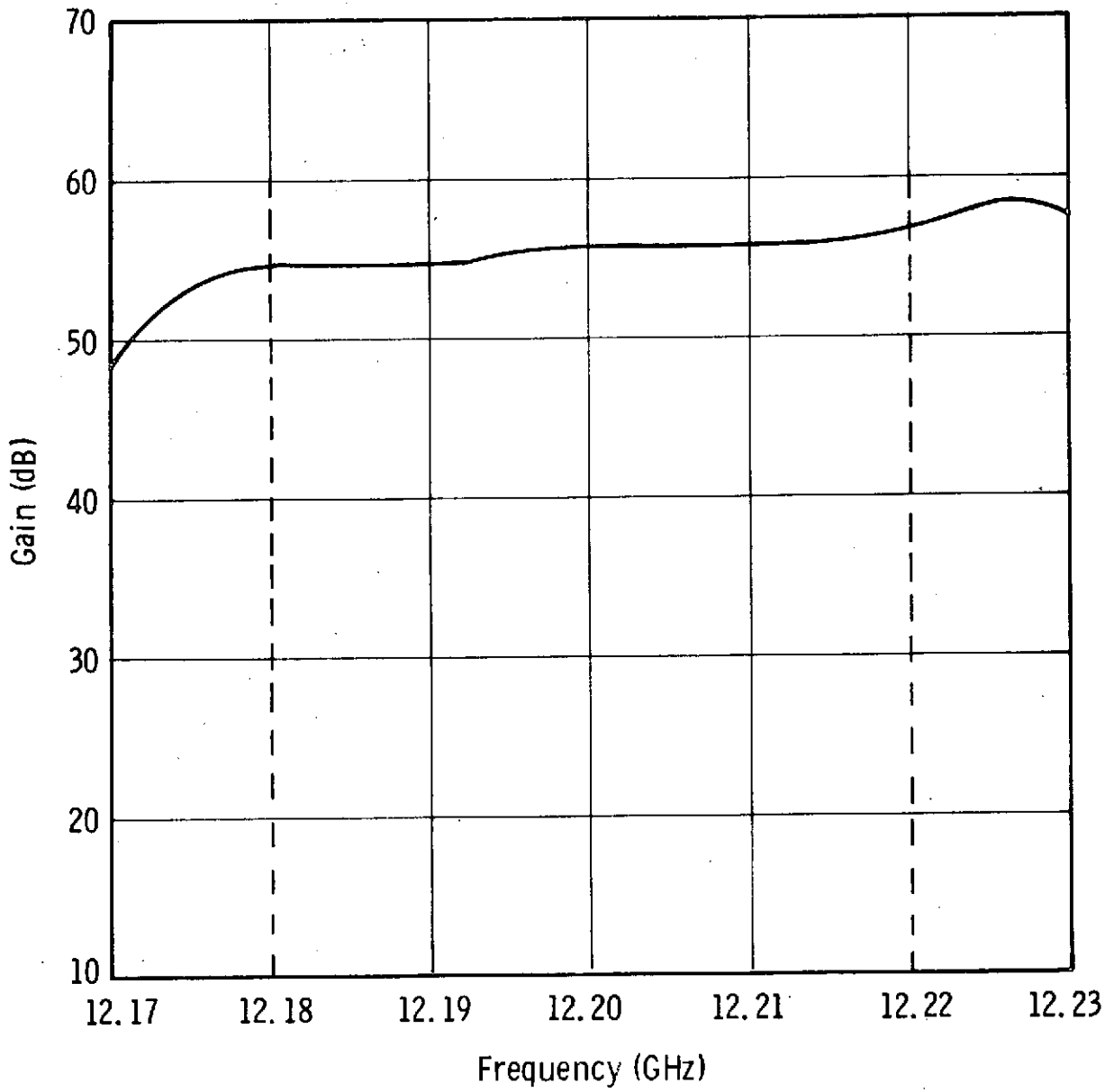
Figure 4-3. Computed Small-Signal Gain as a Function of Frequency
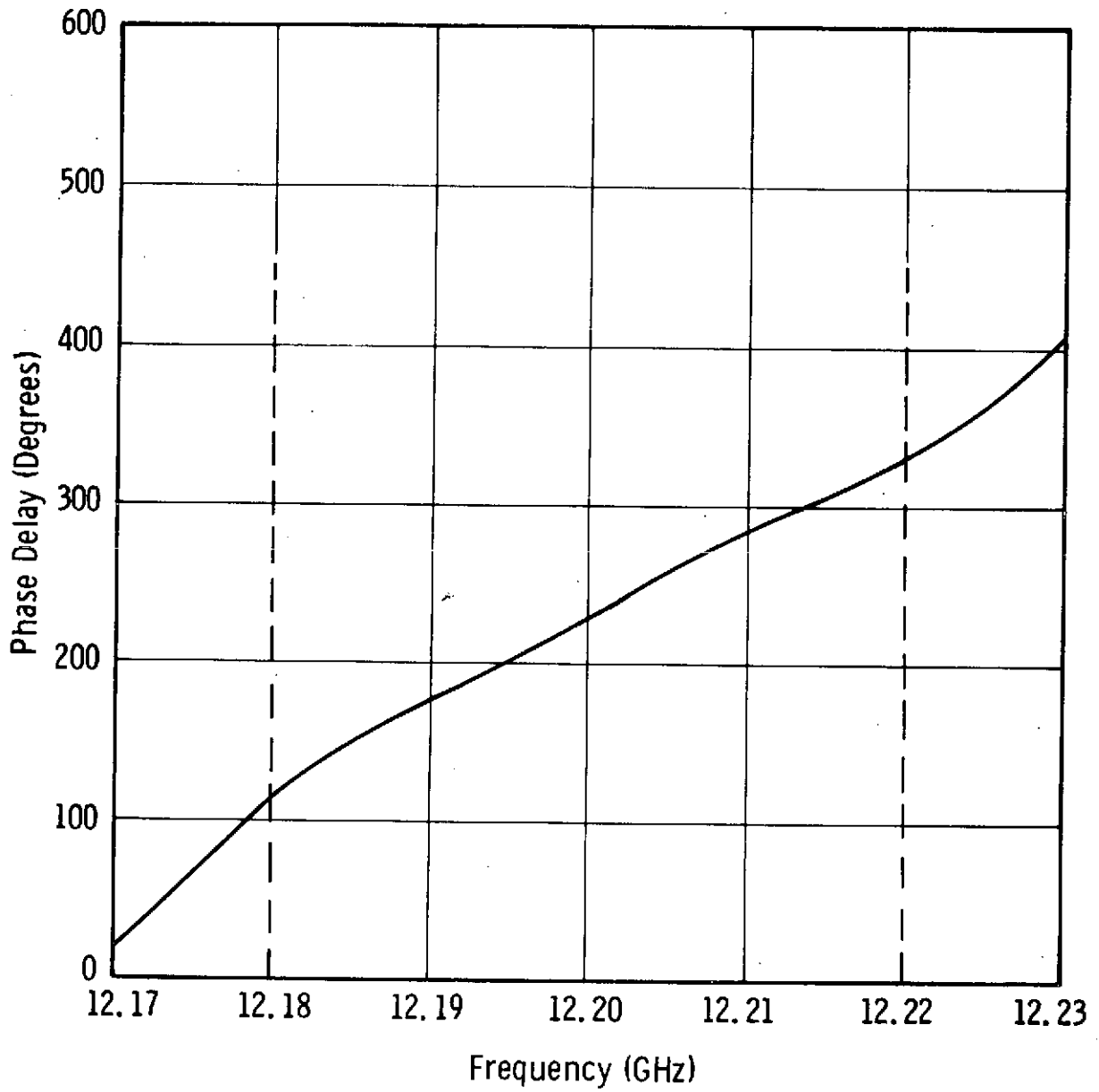
TP A-9206
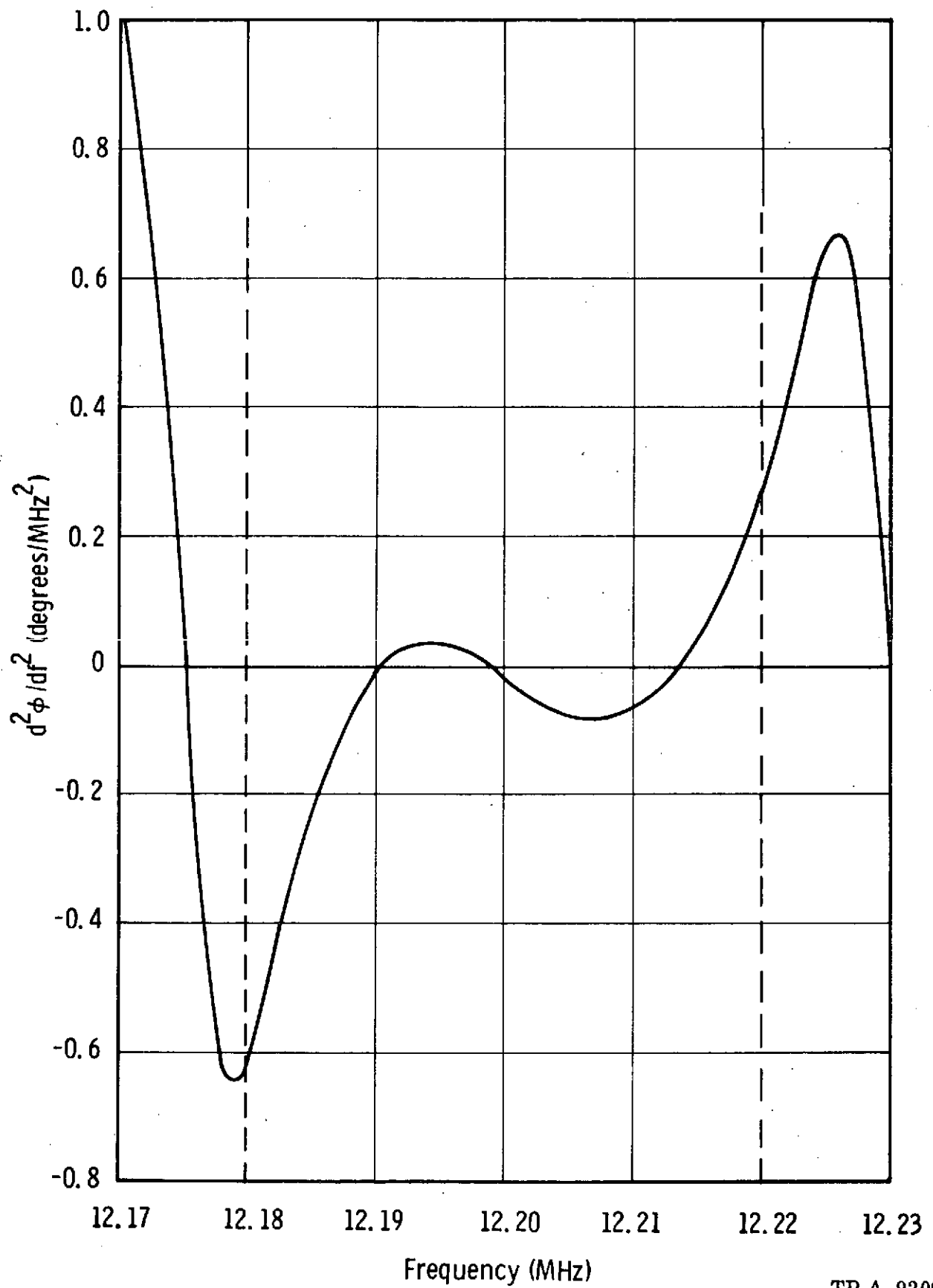
Figure 4-4. Computed Phase Delay vs Frequency

TP A-9208

Figure 4-5. Calculated Deviation from Linear Phase Shift vs Frequency

19

Figure 4-6. Calculated $d^2\phi$ (w)/dw^2 as a Function of Frequency

TP A-9209

4.3 Gun and Beam Analysis

The electron gun is of the type commonly called "convergent confined flow" but perhaps more accurately named "space charge balanced flow." The object of the design is to obtain a beam which is laminar and unscalloped and maintained in equilibrium with a magnetic focusing field approximately 2.5 times the Brillouin field.

One procedure used to design electron guns for space charge balanced flow starts with an electrostatic gun design which produces a highly laminar beam of uniform current density with minimum beam radius equal to the desired final beam radius. If a magnetic field can be found which has flux lines which exactly follow the electrostatic beam trajectories from the cathode to the beam minimum, then the application of this magnetic field will not perturb the electron trajectories. If, at the electrostatic beam minimum, the magnet field can be made to abruptly increase, then all the conditions for space charge balanced flow will have been met. While it is not possible to abruptly change the magnetic field, it is usually possible, in practice, to find a field shape which produces the same effect.

An alternative design procedure starts with an electrostatic gun which produces a beam having a minimum radius slightly larger than the desired beam. A magnetic field is applied, the flux lines of which are tangent to the electron trajectories at the cathode, but which converge very slightly more rapidly than the electrostatic trajectories. The resultant magnetic forces cause a slight adiabatic compression of the beam and, when properly implemented, can produce a relatively scallop-free space charge balanced beam.

The computer aided design procedure for the electron gun comprises the following steps:

1. A trial gun is designed based on Pierce (Ref. 7) theory or on existing gun designs.

2. A computer run of the electrostatic trial gun is made to determine whether this gun will produce an adequately laminar beam of the correct perveance and convergence.

3. Adjustments are made and the gun is recomputed until a satisfactory electrostatic beam is produced.

4.   A polepiece configuration which will produce the desired magnetic field shape is derived from design curves which have been produced by the solution of Laplace's equation for a large number of polepiece configurations.

5.   Beam trajectories are computed for the gun in the presence of the chosen magnetic field.

6.   Adjustments are made, if needed, until the computed beam trajectories satisfy the requirements of the design.

7.   The computer designed gun is tested in the beam analyzer. Further modifications to the design are made, if needed, to bring the gun up to the required performance levels.

The computed electrostatic beam trajectories for the final trial gun design are shown in Figure 4-7. This design shows good laminarity and a minimum beam diameter of 0.033 in. The computed perveance is 0.533 μperv and the maximum cathode loading is 2 A/cm^2. The computed inter-electrode voltage gradient is shown in Figure 4-8, indicating a maximum gradient of 190 kV per inch.

After several trial runs in the beam analyzer a polepiece configuration was found which produced the results shown in Figure 4-9. This figure shows a sequence of cross sections of beam current density as the beam proceeds downstream from the anode. The gun has been scaled-up in size in order to increase the accuracy of measurement in the beam analyzer. Beam scalloping is 11%.

The goal curve for the magnetic field in the region of the cathode is shown in Figure 4-10. Superimposed over this goal curve is the magnetic field actually achieved with the polepiece design for the first tube.

The electron beam is required to exit into a magnetically field-free collector. The maximum collector field at a position two exit hole diameters beyond the collector polepiece face must be less than 0.5% of the focusing field.

22

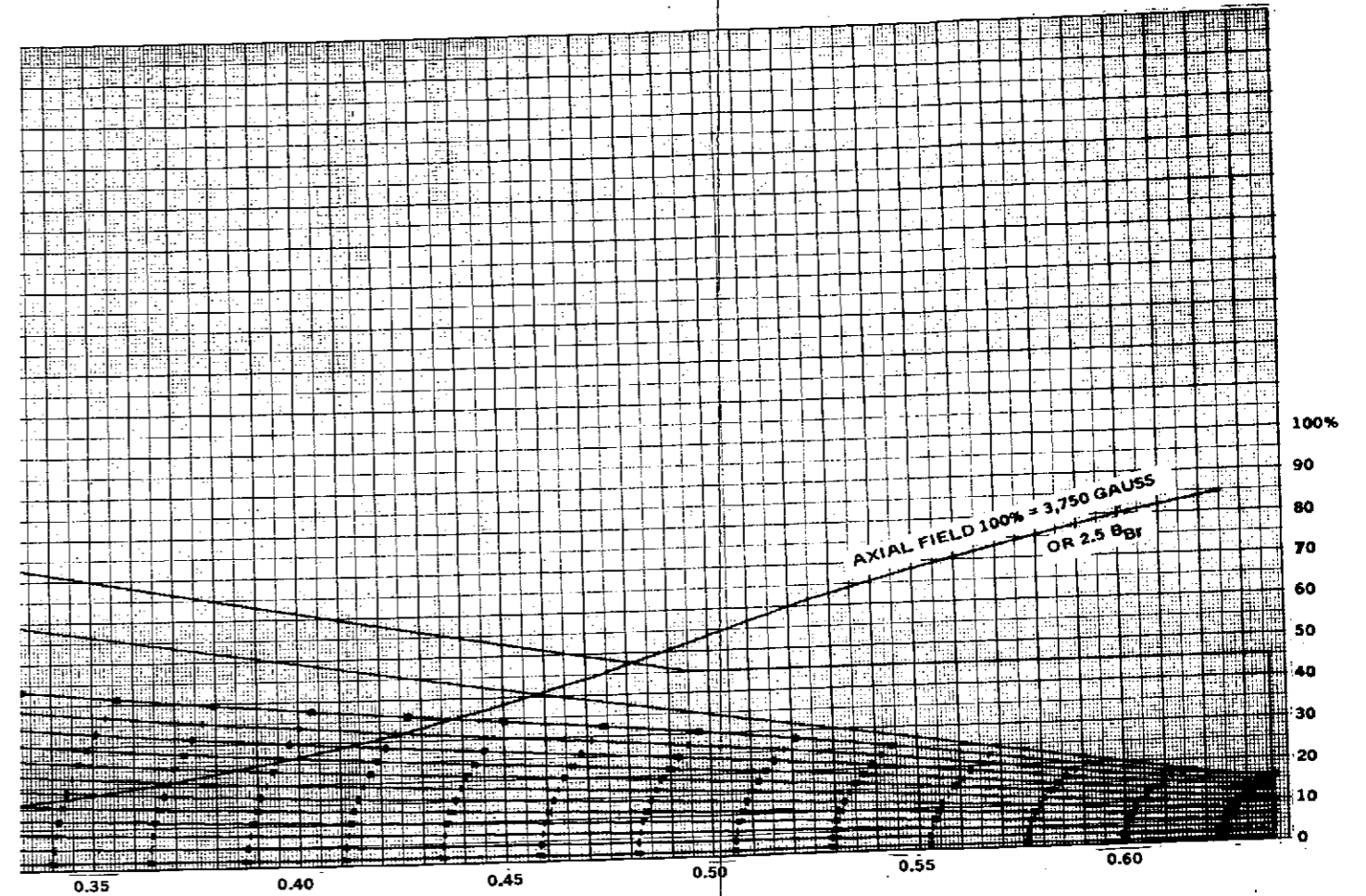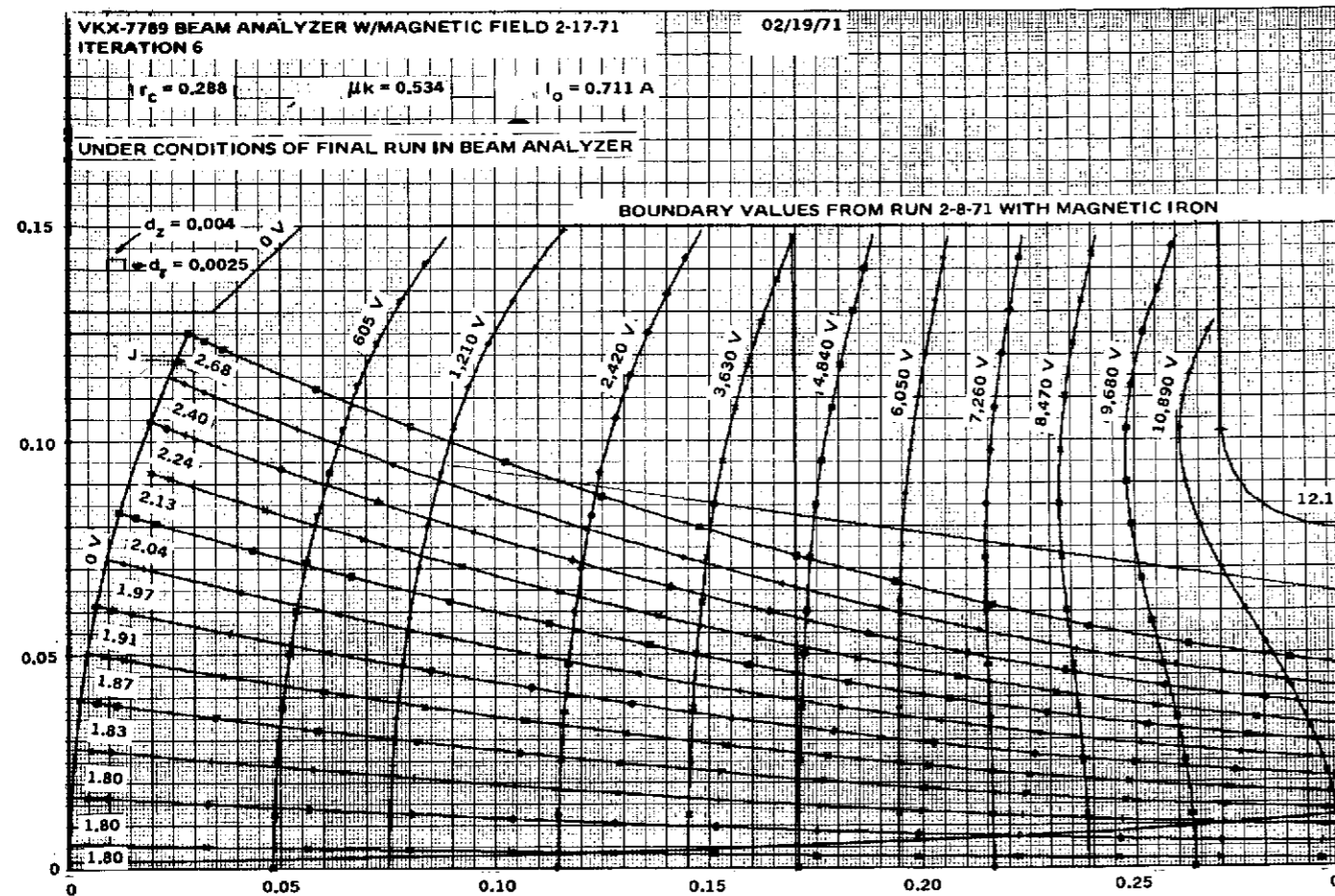Figure 4-7. Computed Electrostatic Beam Trajectories for Final Trial Gun Design

23
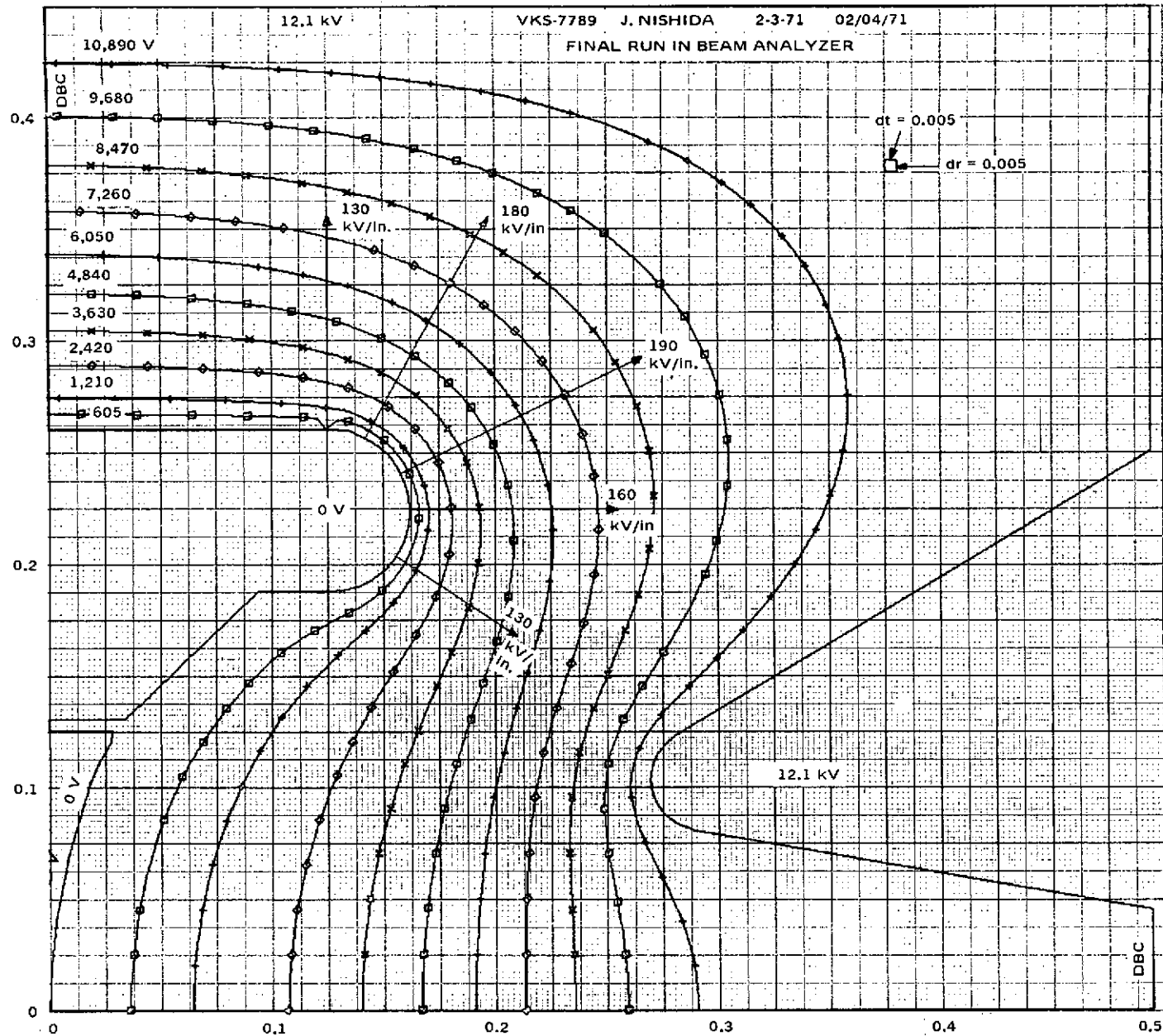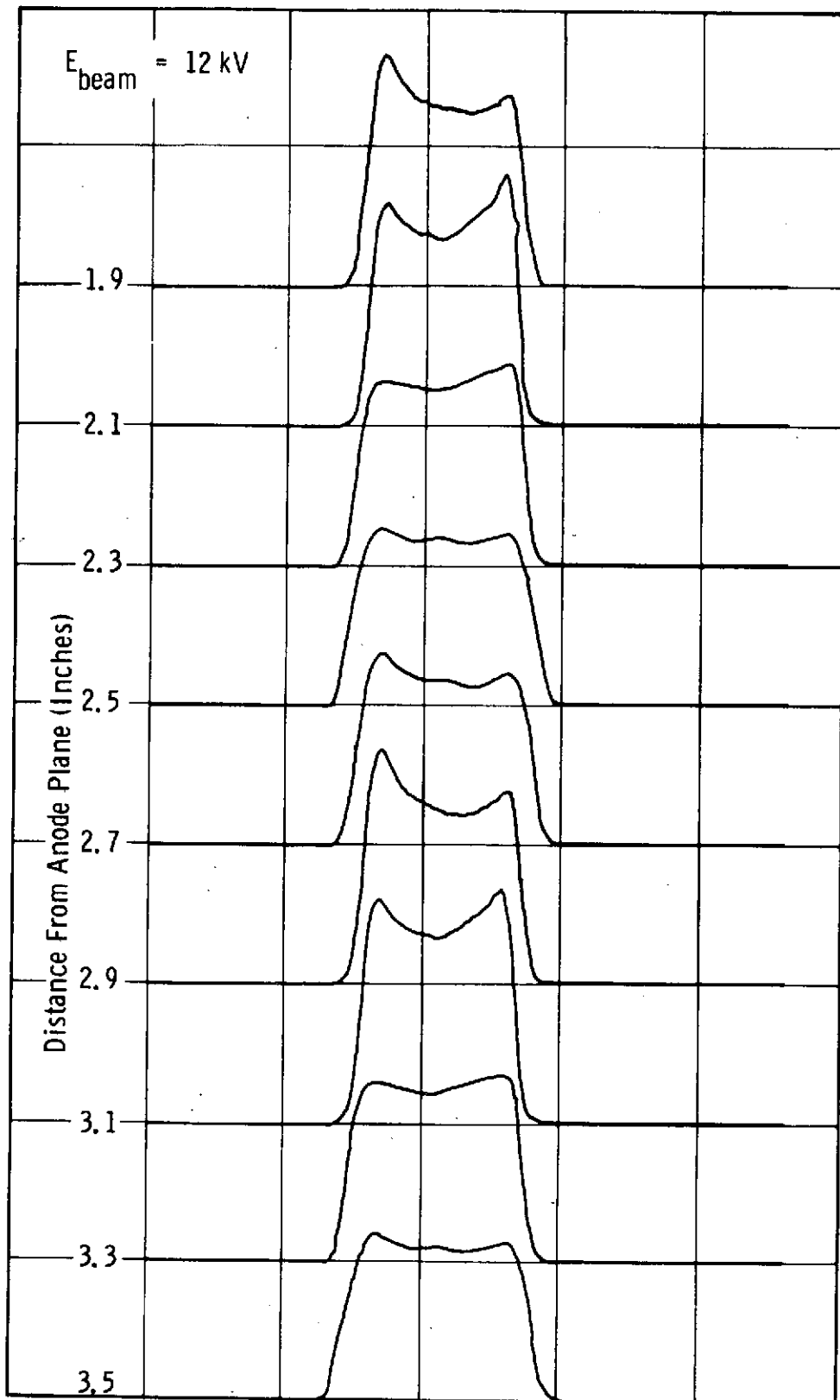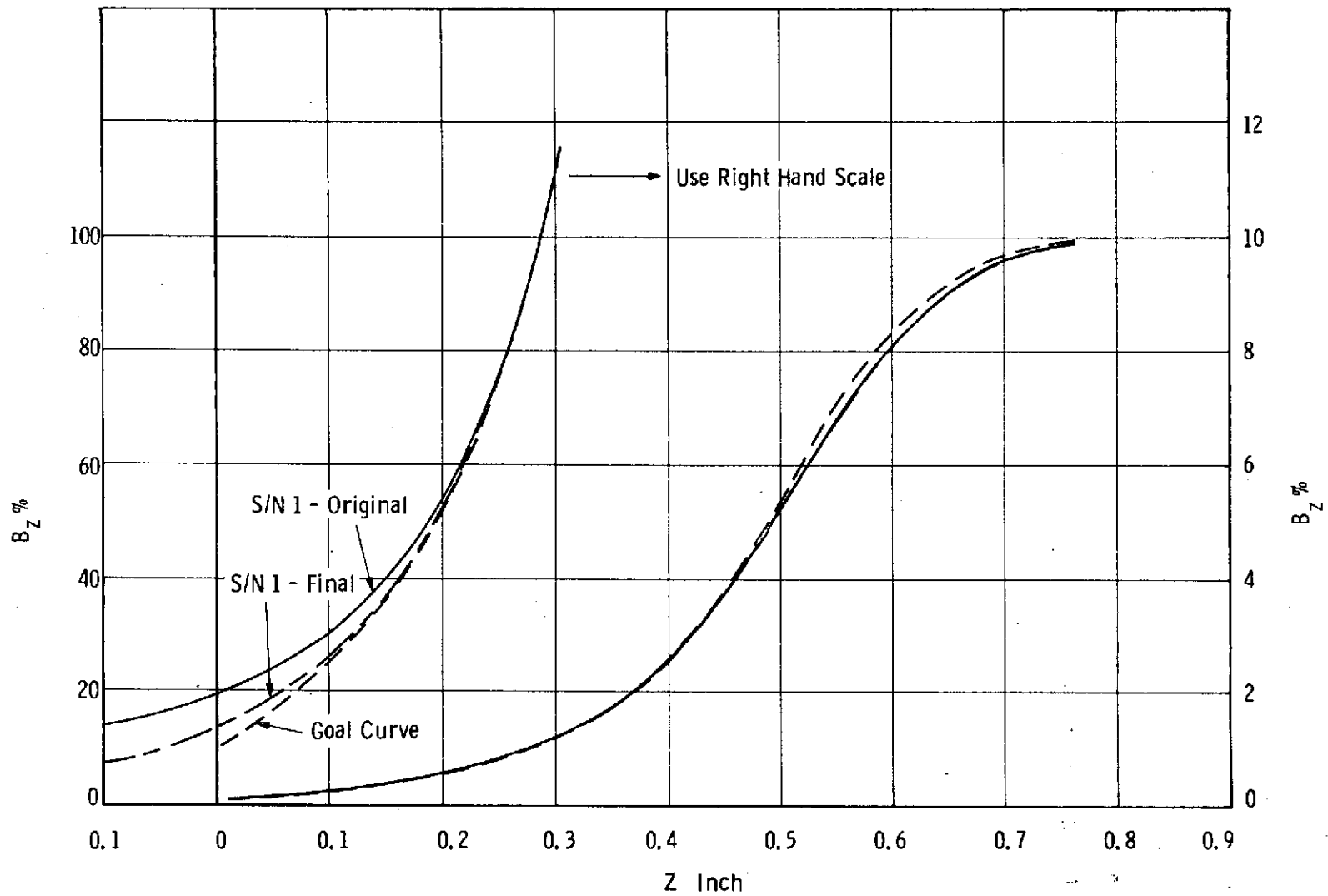
Figure 4-8. Computed Inter-Electrode Voltage Gradient

Figure 4-9.   Beam Current Density Profile vs Distance

TP A-9210

26

Figure 4-10. Goal Curve for Magnetic Field in Cathode Region (Left Curve
is 10X expansion)

TP A-9211

The inner collector polepiece configuration and the resulting measured axial magnetic field is shown in Figure 4-11. This polepiece configuration produces a maximum collector field less than 0.2% of the focusing field. No other magnetic shielding is required to meet the specification.

Figure 4-12 shows the computed electron beam trajectory in the collector for this field configuration, along with the calculated power dissipation profile. The maximum power density of 2.75 kW/in^2 occurs in the well-cooled center section of the collector.
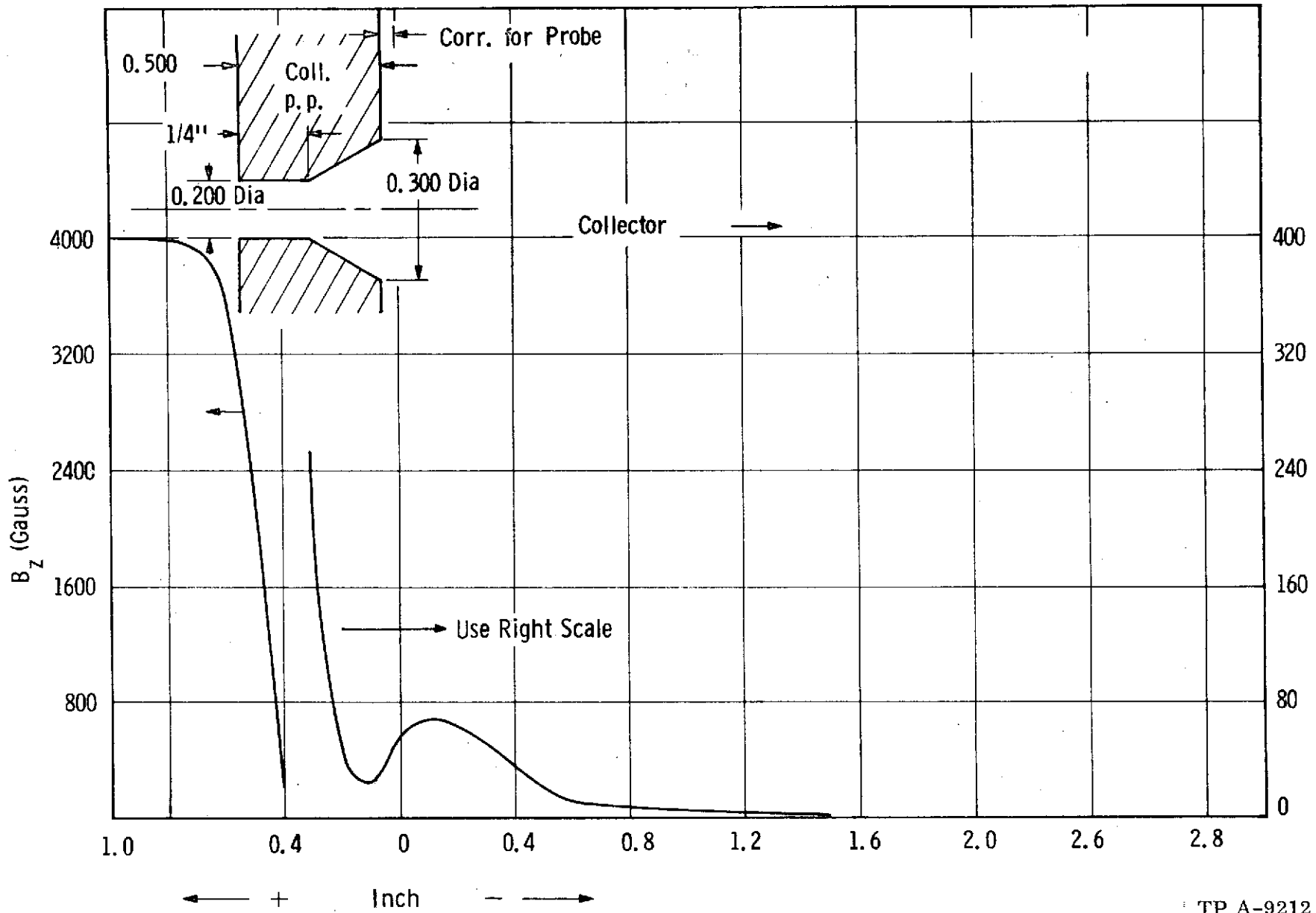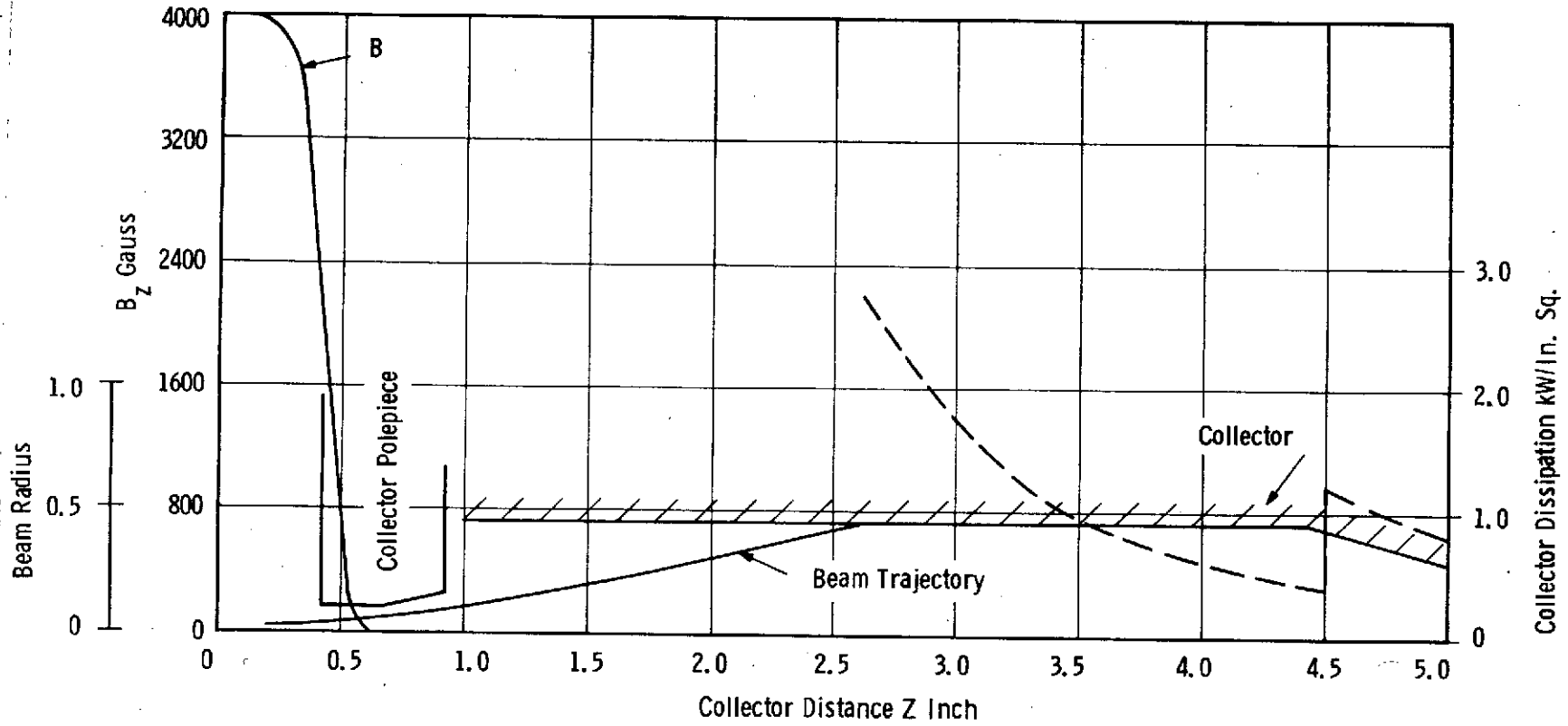
Figure 4-11. Collector Leakage Field

TP A-9212

Figure 4-12. Computed Electron Beam Trajectory in Collector and Calculated
Power Dissipation Profile

TP A-9213

5.0 MECHANICAL DESIGN

The mechanical design of the VKX-7789 resembles that of many other Varian klystrons at this general frequency range. The major departures from conventional design are brought about by the requirement that this tube be operable inside a space-simulating vacuum chamber. It is necessary to provide a removable collector which, for experimental purposes, is to be replaced by a multistage depressed collector for efficiency enhancement studies.

The electron gun is also required to be demountable so that it may be replaced.

The focusing solenoid is also unusual in that it must be capable of being baked out so that the system may be evacuated to the pressure levels appropriate to klystron operation.

Figure 5-1 is the outline drawing of the tube mounted in its focusing solenoid.

5.1 RF Body Construction

The buncher cavities are milled out of a solid copper block with thin copper diaphragms brazed onto the open ends. The diaphragms are connected to a tuner mechanism for final trim tuning under hot test. A cross-sectional view of a typical driver cavity is shown in Figure 5-2.

The output cavity on the first tube was of toroidal configuration (Figure 5-3) with an electro-polished surface finish of 25 microinches, to reduce rf losses to a minimum. This design was changed on the second and third tubes to a milled configuration similar to the driver cavities, because of the thermal drift problems found on the first tube.

Water cooling of the body block is accomplished through a series of transverse cooling passages drilled through the web between cavities. The space available between the penultimate and output cavities did not permit cooling of that area, which eventually proved to aggravate the thermal drift of the first tube.
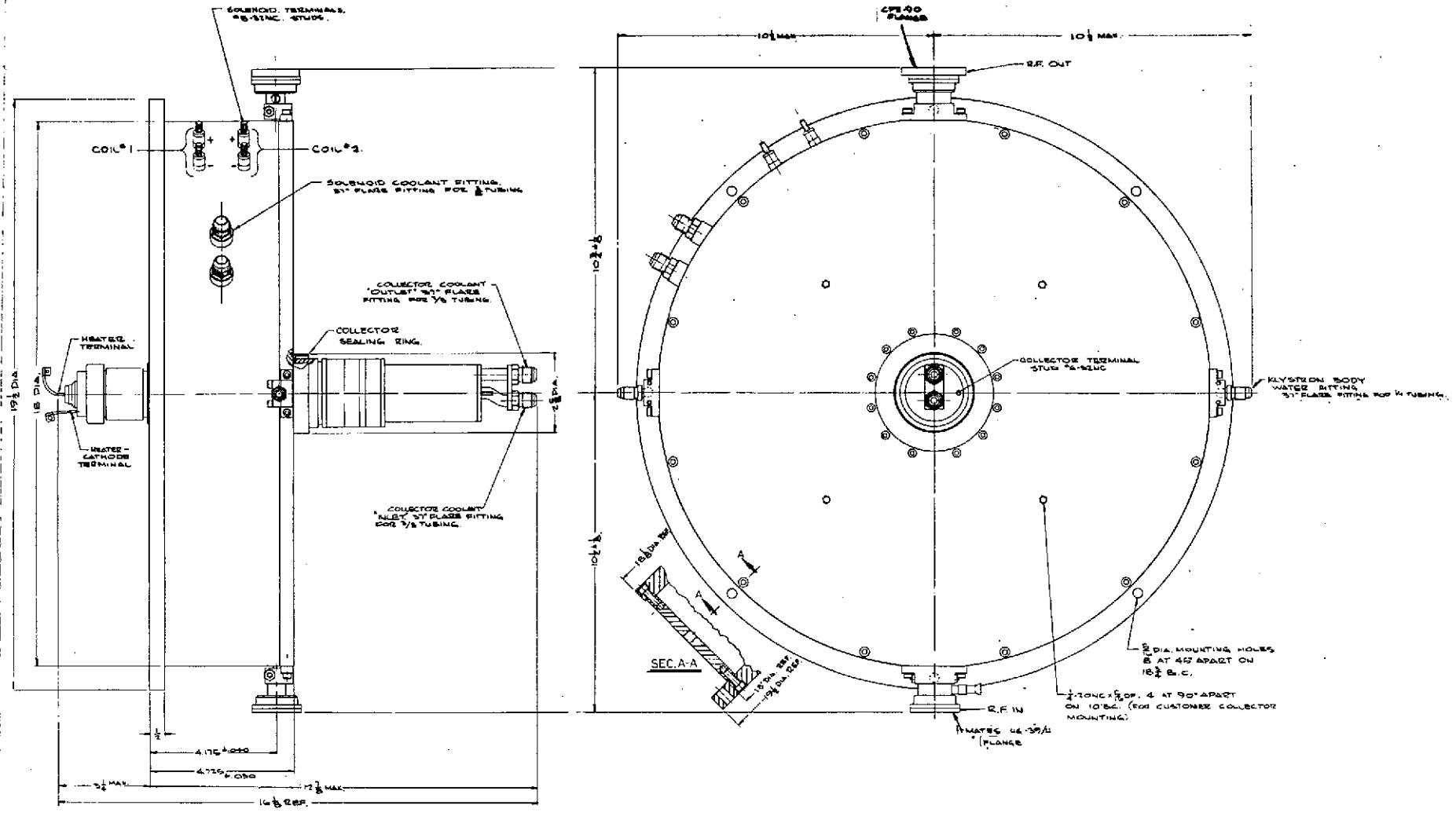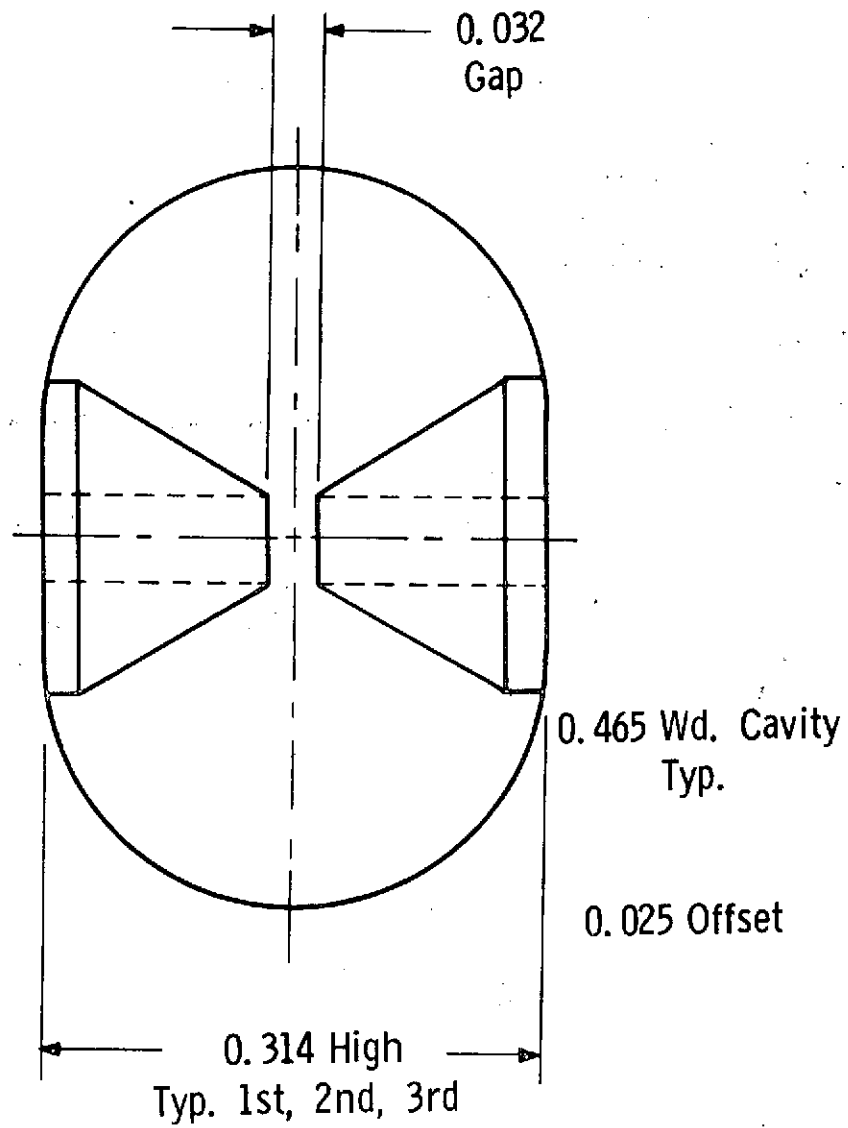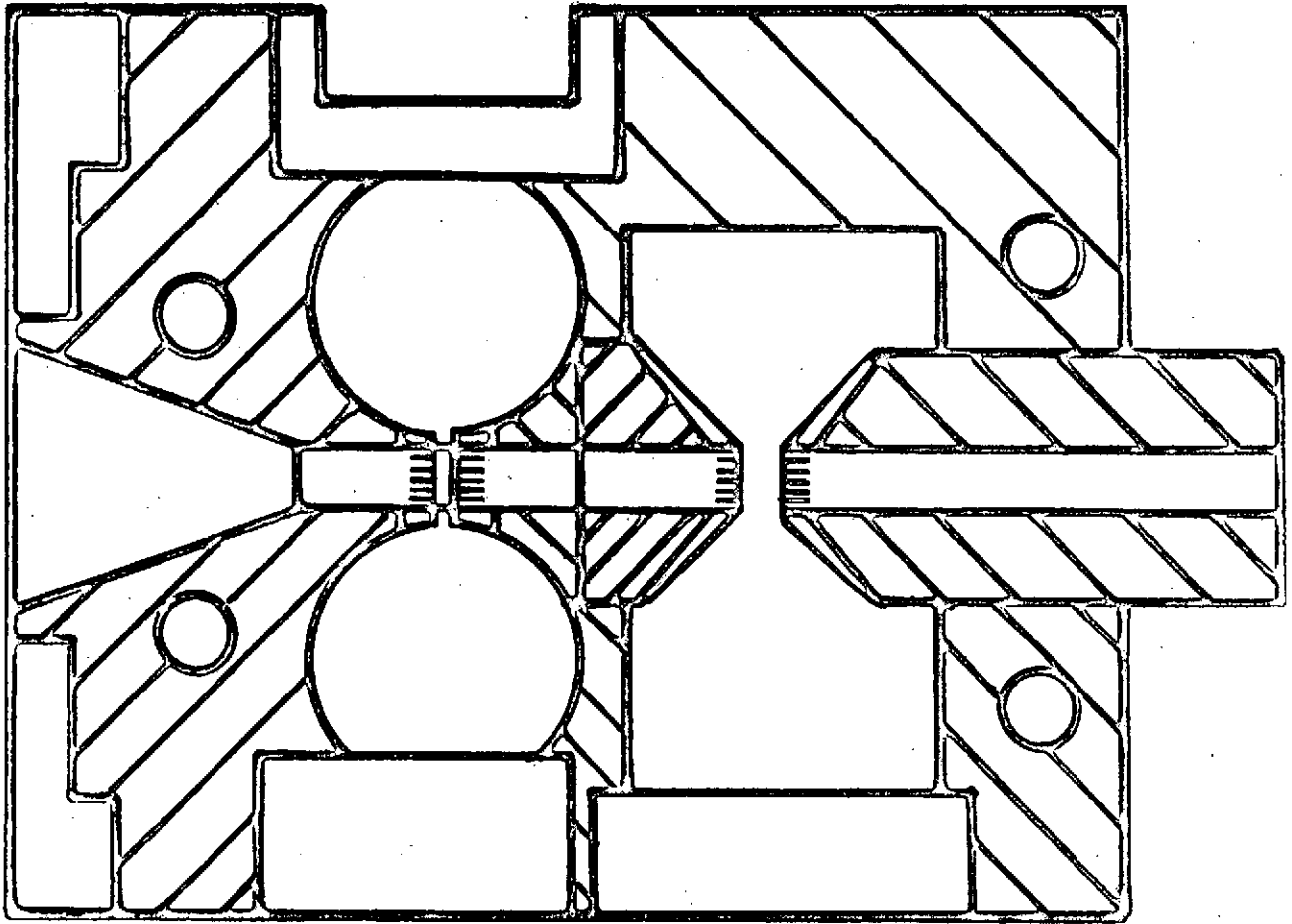
Figure 5-1. Outline Drawing of Tube Mounted in Focusing Solenoid

0.032
Gap

0.465 Wd. Cavity
Typ.

0.025 Offset

0.314 High
Typ. 1st, 2nd, 3rd

TP A–9214

Figure 5-2.   Cross-Sectional View of a Typical Driver Cavity

Figure 5-3. Toroidal Configuration of Output Cavity on First Tube

The input and output coupling is by way of WR-90 waveguide through a pillbox-type ceramic window, through a step-transition to half height waveguide, and through appropriate waveguide bends terminating at the input and output cavity coupling irises. The input and output waveguides are brought out at the collector end of the tube body in such a manner as to allow the tube to be inserted into the focusing solenoid while avoiding interference with the experimental depressed collector. Radial extensions of both input and output waveguides are required so that the waveguide windows can clear the outer diameter of the solenoid.

Gun and collector polepieces made of soft iron are brazed to the body assembly, and are sized to mate snugly with the solenoid, thereby completing the magnetic circuit.

The final body configuration is shown in Figure 5-4.

5.2 Collector Construction

The collector is of conventional design, taken from a 10 kW klystron. It is supported by a ceramic insulator in order to allow measurement of beam transmission.

The major feature of the collector design is the heliarc flange by which it is mounted to the collector polepiece. This is designed to provide maximum unimpeded access to the beam exit tunnel upon removal of the collector. This feature can be seen in Figure 5-5.

5.3 Electron Gun Construction

Figure 5-6 shows the demountable electron gun. The gun ceramic support cylinder is made large in order to minimize leakage in a less than optimum environment. The cathode employed is a dispenser cathode, because an oxide coated cathode could not be expected to provide the cathode current density required in this application. The cathode is supported by a conical sleeve which is attached to the inside of the focus electrode support sleeve. This assembly is brazed to a heavy support ring which is attached to the base of the gun ceramic by means of six machine screws.
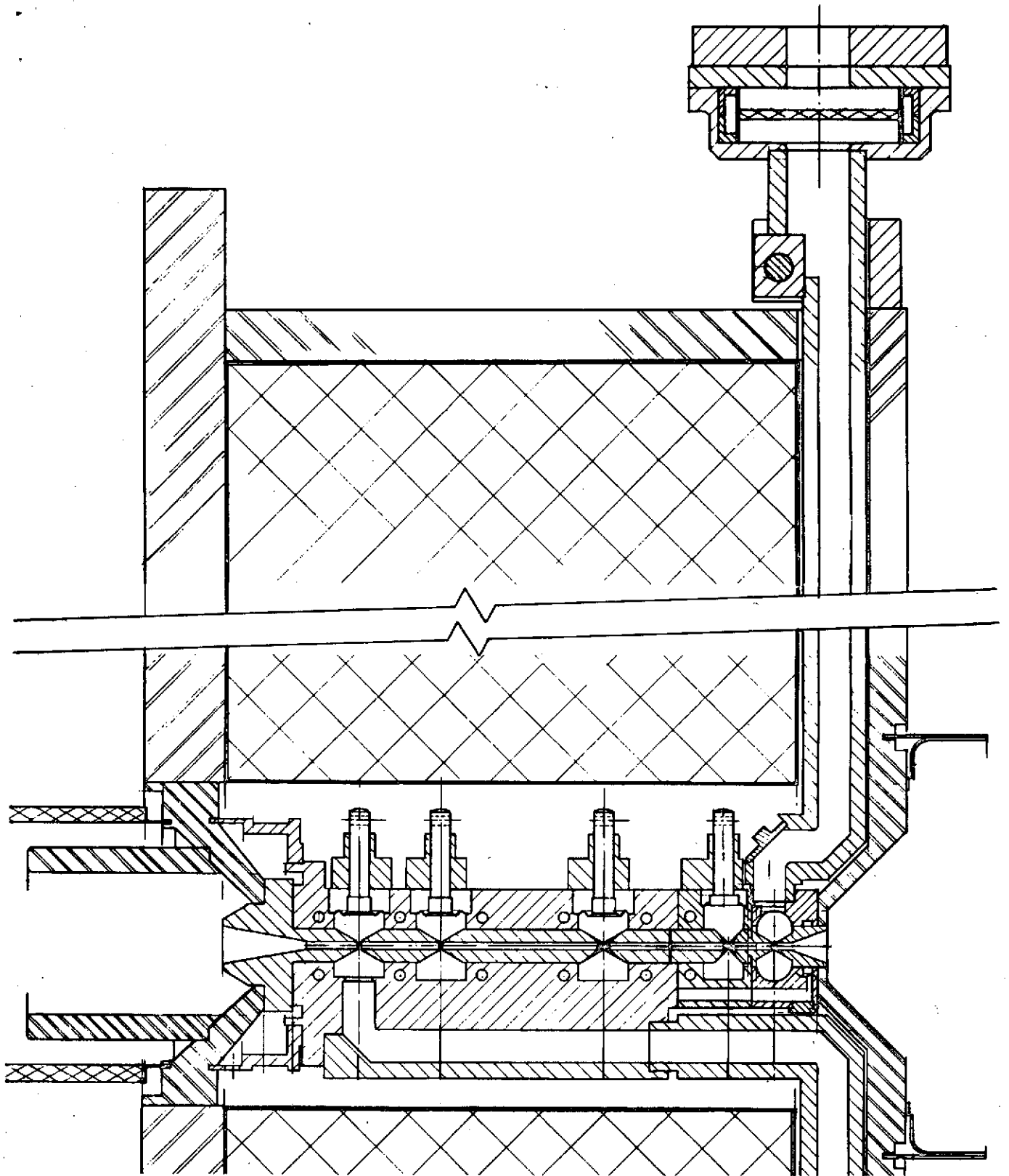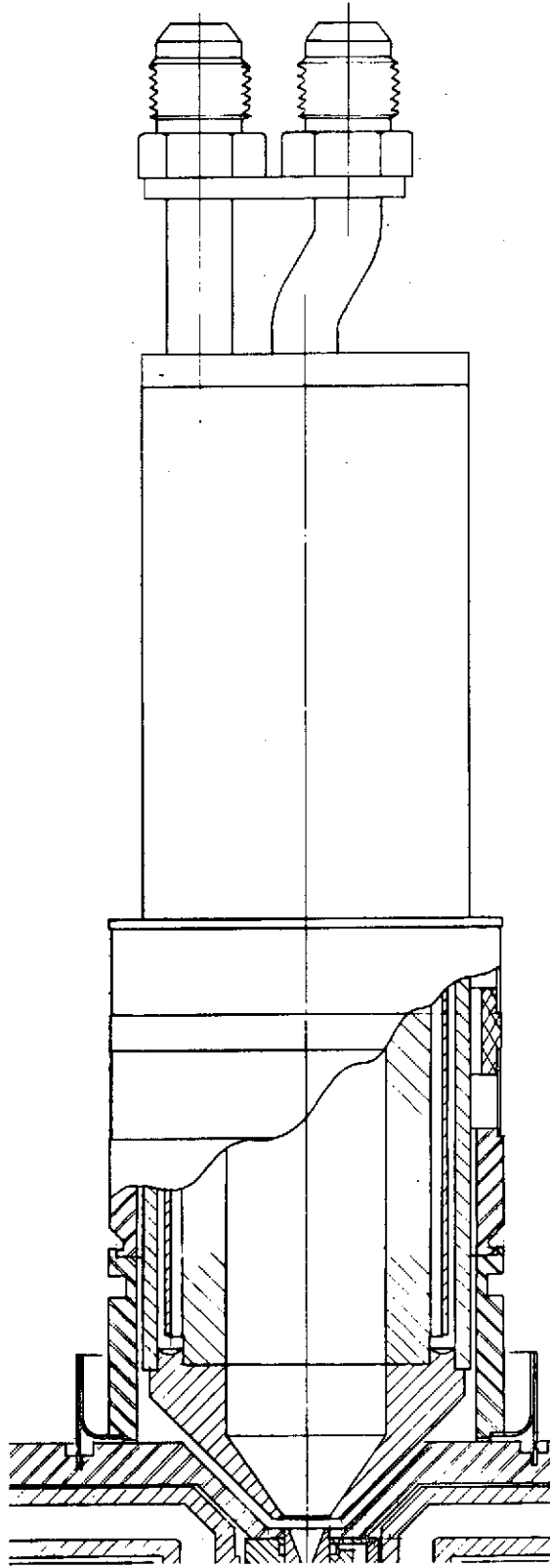
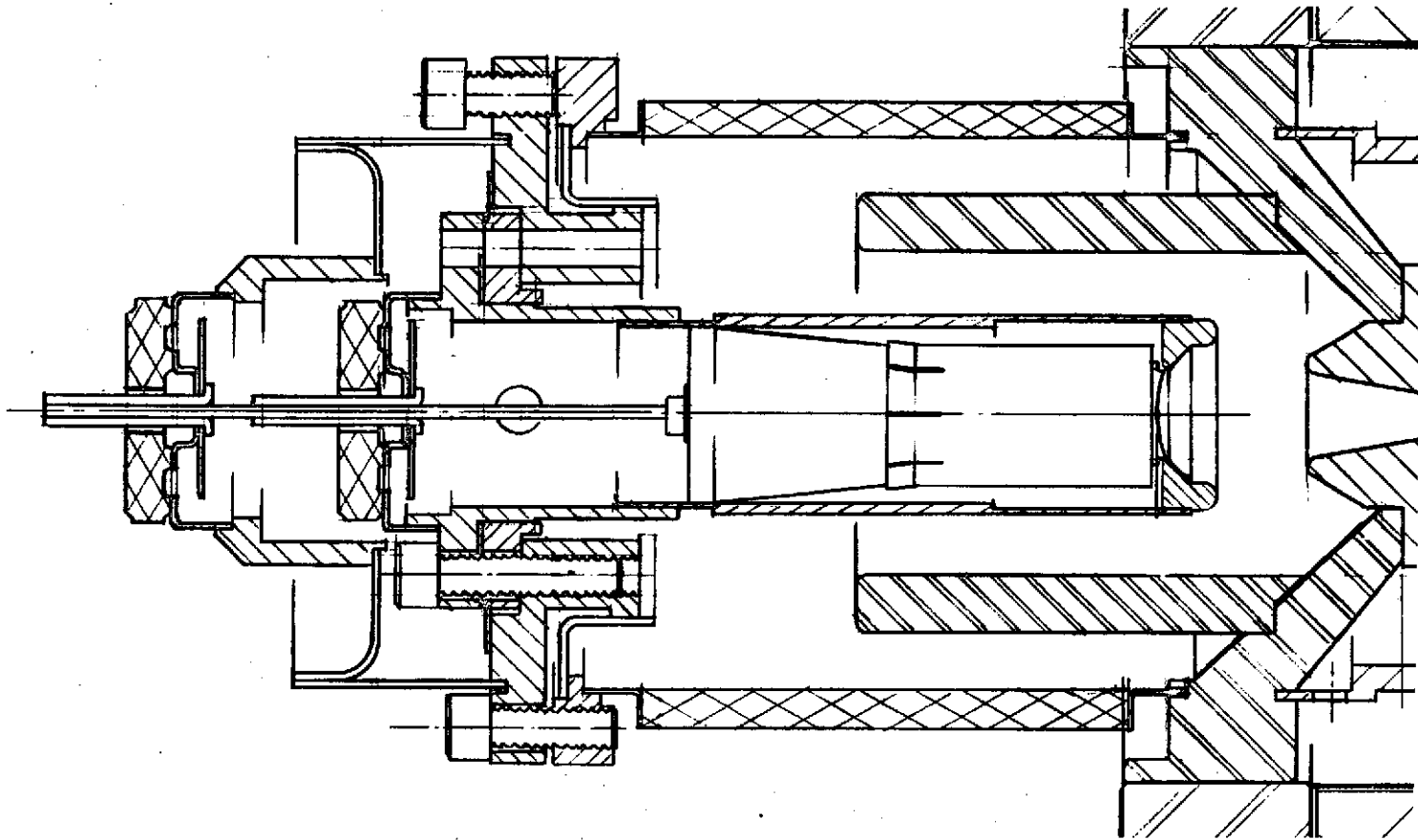Figure 5-4. Final Body Configuration

Figure 5-5. Collector Layout Drawing
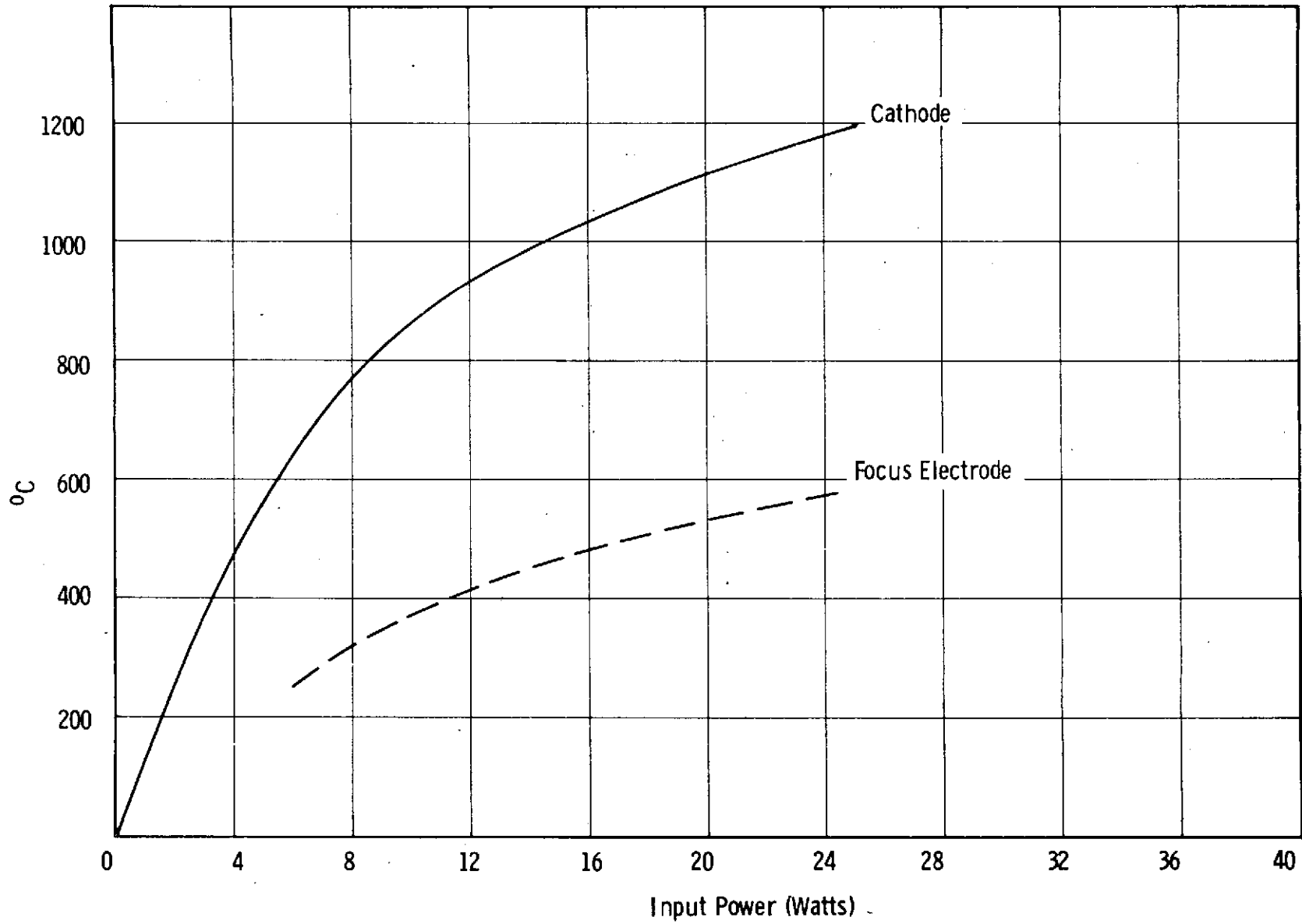
Figure 5-6. Demountable Electron Gun

Figure 5-7. Cathode Temperature vs Input Power.

TP A-9216

The original gun vacuum envelope is completed by a secondary feed-through structure that is heliarc welded to a sleeve at the base of the gun ceramic and to the heater rod. At the time of gun replacement these heliarc joints are cut and the secondary feed-through plate discarded. The new gun can then be mounted in place of the old gun, using the machine screws.

5.4 Solenoid Construction

The focusing solenoid is required to be bakeable in a vacuum chamber to 250°C minimum. The solenoid used in this program has been designed to withstand bakeout temperatures to 300°C. To minimize the evolution of gasses during bakeout, the solenoid is completely free of all plastics or other high vapor pressure materials. The magnet coils are made of aluminum foil insulated with aluminum oxide, formed by anodizing the foil. The coils are insulated from the magnet case and magnet coolant plate with mica. Although the cooling efficiency is relatively poor, the ability of the magnet to operate at high foil temperatures minimizes the need for good thermal contact between the magnet coils and the magnet cooling plate.

The focusing solenoid core, or bobbin, is made of nonmagnetic stainless steel. The solenoid case is made of annealed cold-rolled steel coated with electrodeposited nickel, to avoid corrosion. The bottom plate of the case is made of 1-inch thick material in order to avoid flux leakage in the collector region. The collector polepiece of the tube serves as the magnet top plate, and is also of 1-inch thick material.

The focusing solenoid mechanical and electrical characteristics are summarized in Table 5.1.

TABLE 5.1

FOCUSING SOLENOID APPLICATION DATA

Magnetic Field	4000 Gauss
Current	20 amperes
Voltage (Winding Temperature of 130°C)	105 volts D.C.
Resistance at 20°C	3.46 ohms (max)
Non-operating Temperature	300°C
Coolant	Water
Flow	1.5 gpm
Weight	150 pounds
Length of Magnet	4.5 in.
Inner Diameter	2 in.
Outer Diameter	18 in.

6.0 EXPERIMENTAL RESULTS

6.1 Initial Cold-Test Results

The preliminary cold-test work required for selection of cavity dimensions was done on individually machined copper test sections. Several existing Varian klystrons at similar operating frequencies use the milled cavity approach, where cavities with full-radius sidewalls are milled into a solid copper block. A beam hole is drilled and the drift tubes are brazed in. This technique has the advantage of being simple and precise, and results in a good thermal design.

Nominal tunnel diameter and drift tube gaps were determined in the analytical design phase of the program, and the cold-test design work was aimed at achieving a cavity size that had the proper resonant frequency, good form factor and maximum R/Q.

Figure 5-2 shows a cross-sectional view of the cavity design selected for the first three driver cavities. Using quartz rod perturbation techniques, the measured R/Q of this cavity was 130 ohms. Q_o was 2800.

The coupling aperture for the input cavity is also machined into the copper body block, with the dimensions of the coupling iris determined by the desired Q external of 600. Since the presence of the coupling aperture also detunes the cavity resonant frequency, an adjustment in cavity length was made to re-establish the desired frequency.

The short drift length desired between the penultimate cavity and the output cavity placed a limitation on the length of the downstream drift tube tip. Since the cavity and drift tube size used on the first three cavities would cause this drift length to be too great for good high efficiency performance, the gap in the penultimate cavity was moved offcenter toward the output cavity. This, in turn, lowered the resonant frequency of the cavity to a point where the cavity height had to be reduced (to 0.250 in.) to obtain the desired operating frequency. This modification reduced the cavity R/Q to 120, a value still considered adequate for proper tube gain and bandwidth performance.

43

A copper diaphragm end-wall trim tuner was designed and used on the first four cavities, allowing about ±100 MHz tunability with a total diaphragm movement of 0.040 inch.

The design of the output cavity for the first tube was based on the work described in the results of Contract NAS3-11533 (Ref. 3). In this work it was found that circuit efficiency could be maximized by using a toroidal cavity geometry. A test cavity with this configuration was constructed by using two identical machined halves, as shown in Figure 6-1. Coupling to the cavity was provided through a sidewall iris, giving an external Q of 210.

A study was made of the effect of cavity surface finish on the resultant internal Q factor. Normal fabricating techniques with very careful machining of the cavity surfaces gave a cavity Q_0 of 2600. Further improvement was made by mechanical polishing of the surface with an alumina polishing compound with a particle size of one micron. This gave a Q_0 of 2800. Electropolishing made an additional improvement, with a Q_0 of 3100 for a final surface finish of 8 to 10 micro-inches. This final configuration was used on the first experimental tube.

Except for the length of the required straight waveguide runs, the input and output cavity coupling systems are similar. Two 90 degree mitered bends in reduced height waveguide are used in each line. VSWR versus frequency for the final bend design is shown in Figure 6-2.

The characteristics of the double-step transition from half-height to full-height waveguide are shown in Figure 6-3.

The waveguide window design was based on a pillbox disc window used on several existing x-band klystrons. Several adjustments in both window dimensions and in the pillbox cavity dimensions were required in order to achieve a good match and mode-free performance across the operating frequency band of the tube. The final window match is shown in Figure 6-4.

44

0.051

0.024
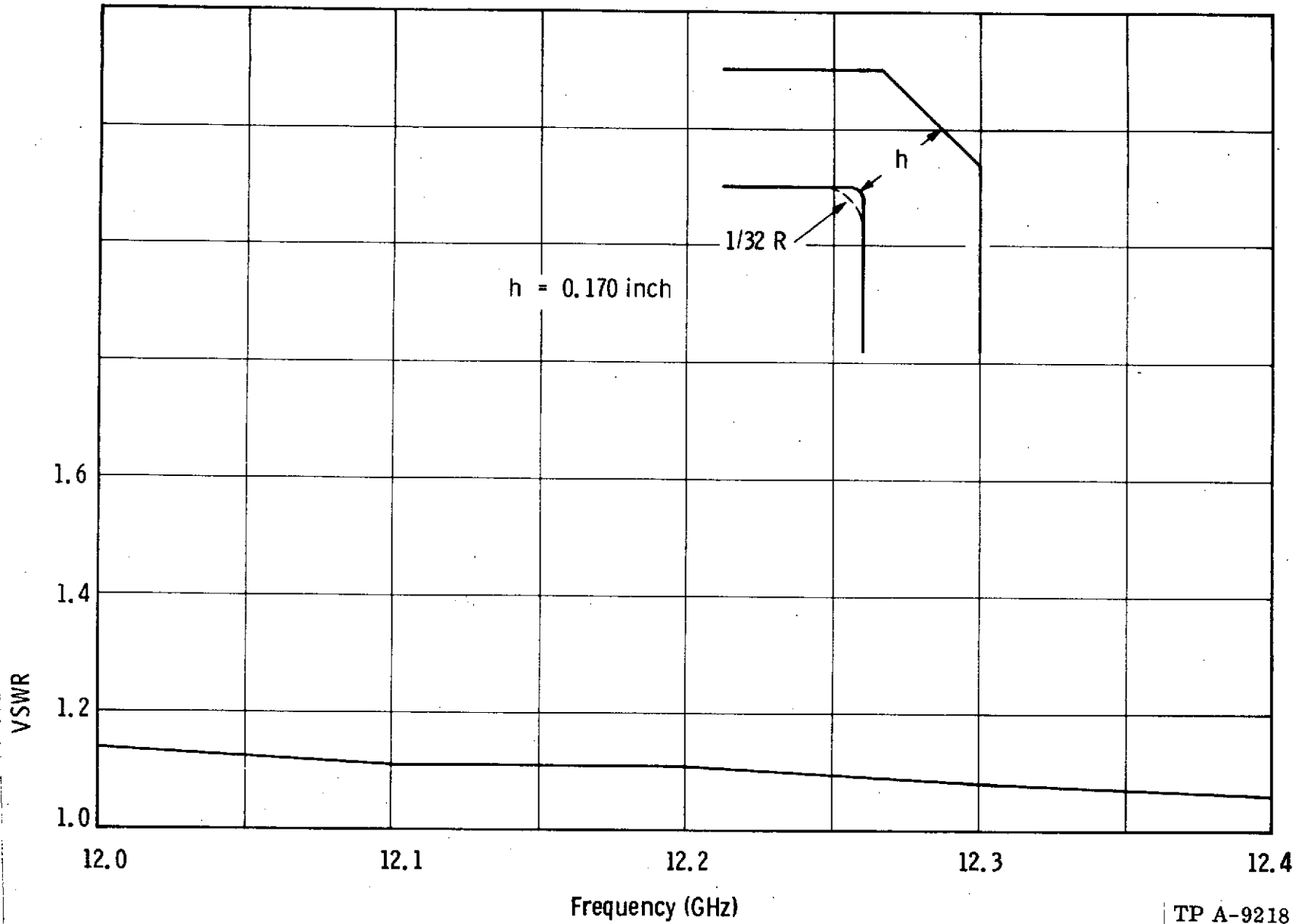Gap
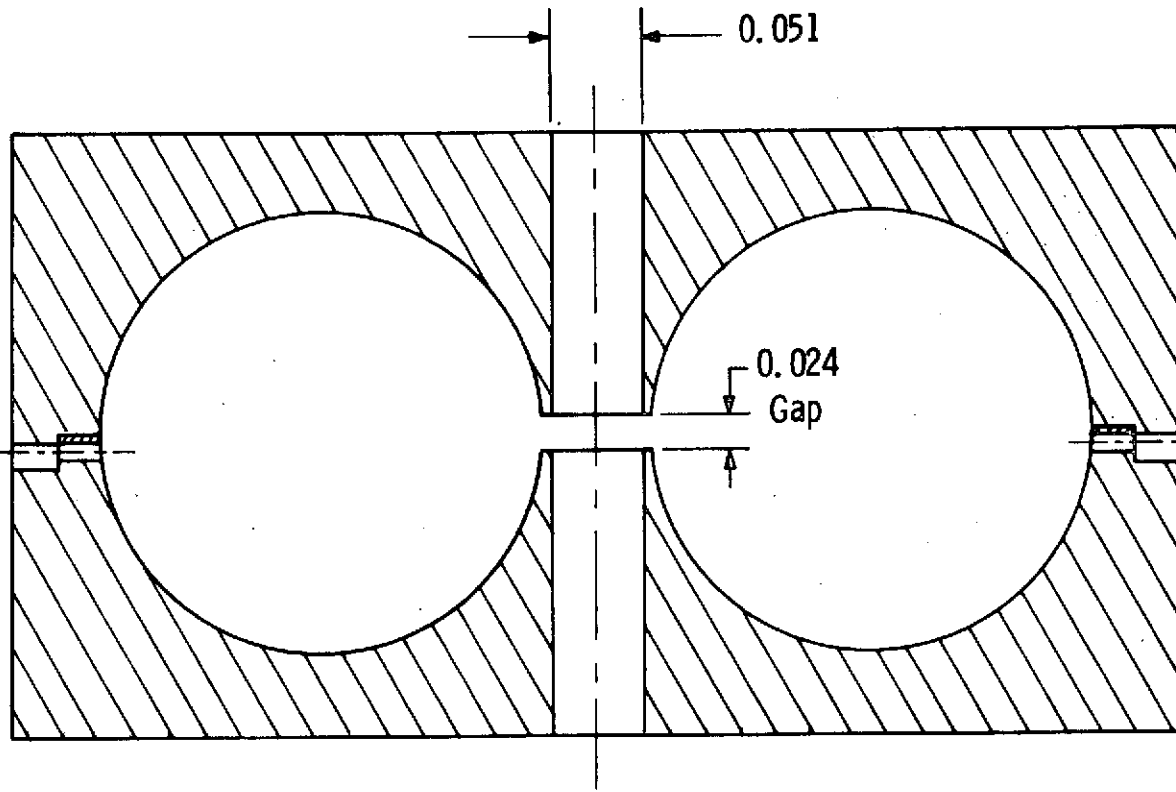
TP A-9217

Figure 6-1. Toroidal Test Cavity

Figure 6-2.   VSWR vs Frequency for Final Waveguide Bend Design
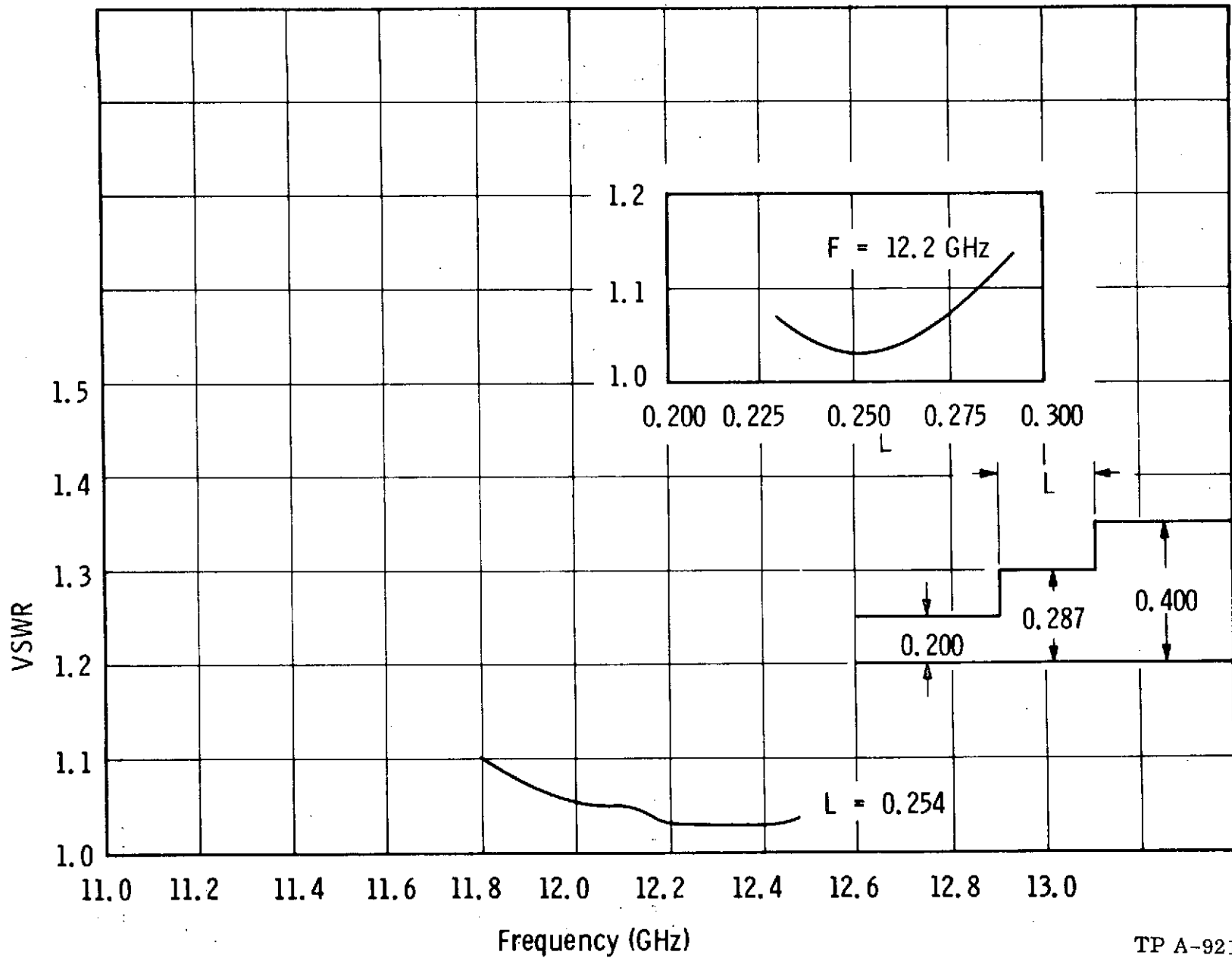
TP A-9218

Figure 6-3. Characteristics of Double-Step Transition from Half-Height to Full-Height Waveguide
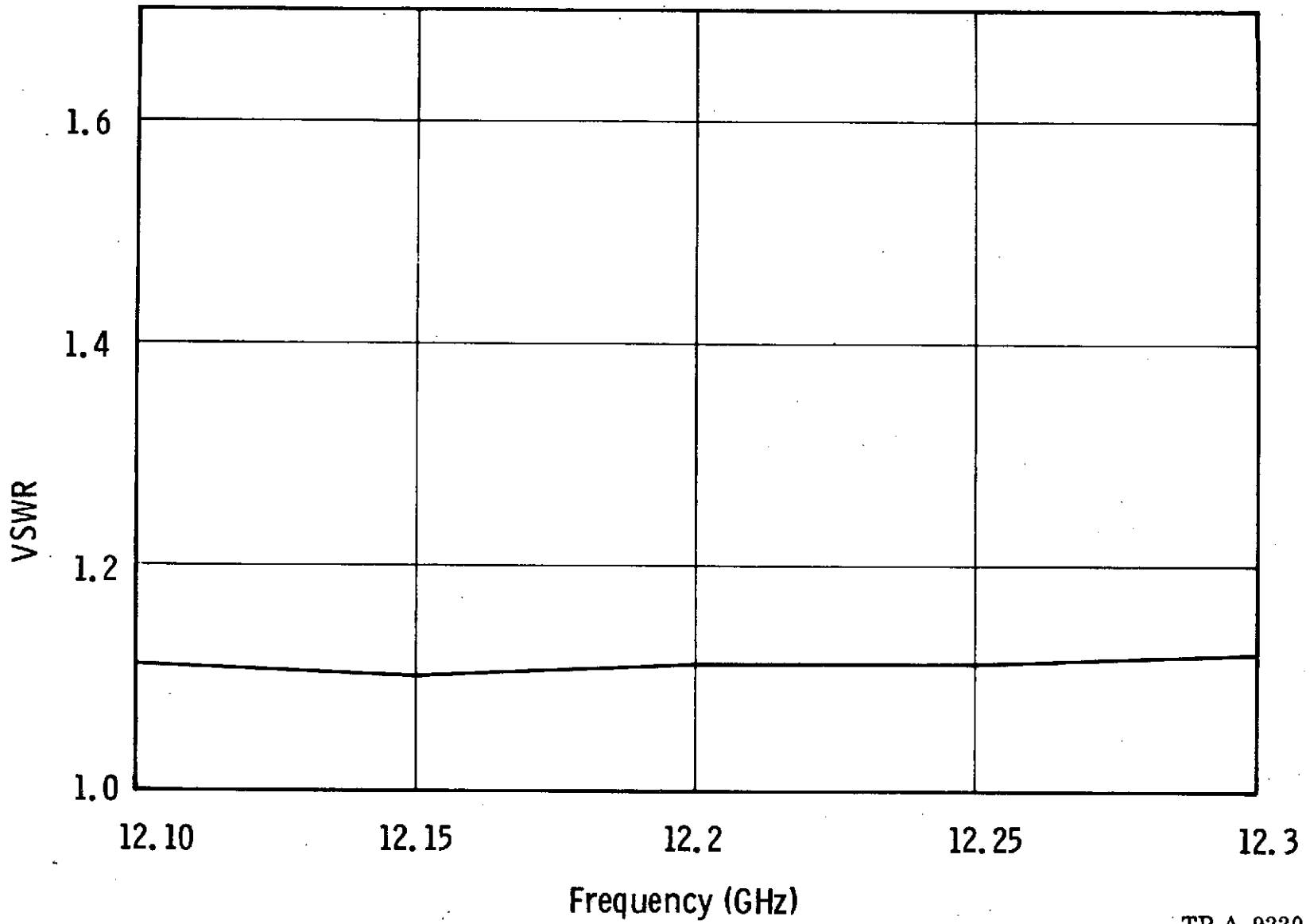
TP A-9219

Figure 6-4. Final Output Window Match

TP A-9220

6.2 Serial Number 1 Test Results

During initial testing of the first tube, it was found that the dc beam transmission was 99.3%. However, the beam transmission under rf operation was very poor (approximately 50%), requiring that the tube be operated under pulsed drive to avoid the effects of overheating during analysis. Even under pulsed conditions, the high body current caused thermal drift of the cavities and stable operation was difficult. Test results at two different beam voltages and duty cycles are listed in Table 6.1.

TABLE 6.1

TEST RESULTS ON SERIAL NUMBER 1

Beam Voltage	10	12	kV
Beam Current	0.505	0.66	Amps
Power Output (peak)	2.78	3.9	kW
Power Output (average)	336	390	Watts
Body Current (average)	30	32	mA
Body Current (peak)	248	320	mA
Efficiency	55	49	%
Dc Beam Transmission	99.3	99.3	%
Perveance	0.505×10^{-6}	0.505×10^{-6}	--
Duty Cycle	12.1	10	%

The maximum efficiency obtained was 55% and occurred at a beam voltage of 10 kV. At the design voltage of 12 kV, the efficiency decreased to 49%, indicating a possible output coupling problem. In order to verify whether this was the case, a variable mismatch was placed between the tube output terminals and the matched waveguide load. Testing was started at low beam voltage and duty. At 6 kV and approximately 200 watts average output power, the tube suffered a loss of vacuum. The VSWR of the mismatch was 3:1. A vacuum leak was found in the output window, due to a failure in the ceramic-to-metal seal rather than a crack in the ceramic itself.

During subsequent analysis of the failed tube, the external Q of the output cavity was measured and found to be 250 instead of the design value of 200. This was probably due partly to the resonant

frequency of the output cavity being 12.1 GHz, instead of 12.2 GHz, and partly to a buildup of assembly tolerances.

A detailed investigation was also made to determine the cause of the unexpectedly high beam interception. The gun and collector were removed and dimensional measurements taken to determine the alignment of the gun, drift tubes and polepieces. The overall alignment appeared satisfactory and was not considered to be a major factor in causing the high body current.

The transverse magnetic field in the solenoid was measured and found to be 0.1%. The tube polepieces were inserted and the transverse magnetic field at the cathode was found to be 2.5%. This was higher than desired and would cause scalloping of the beam. The measured axial magnetic field in the gun was 1.3%, compared to the design value of 1.0%. This would cause additional scalloping and a larger beam. The larger beam diameter would cause higher interception and would also increase the normalized drift lengths, which in turn would cause the maximum efficiency to occur at a lower beam voltage.

Prior to the tube failure, the rf body and output cavity water-cooling circuits were isolated to determine where the body interception was occurring. A significant amount of the power was in the exit drift tube leading to the collector. This was due to the extremely rapid beam expansion past the output gap during rf operation.

The first tube was rebuilt with several modifications to decrease the high body interception. The exit drift tube was enlarged by machining a larger taper into the output polepiece. Although this would not allow the collector leakage field specification to be met, it was considered an expedient move to provide additional performance information prior to a major redesign of the output section.

The magnetic entrance conditions were improved by removing the gun ceramic assembly, remachining the gun ceramic seat and adding a thicker iron gun shield.

No internal modifications were possible to adjust the output cavity external Q, and it was decided that an external load transformer would be used to adjust the coupling.

Preliminary testing showed an improvement in dc body current of approximately 50%. At 10% rf duty and 12 kV beam voltage, the output power was 3590 watts peak and the average body current was 17.5 mA. The body current was still higher than desired, and thermal drift of the cavities was still observed.

A variable phase mismatch was placed in the output waveguide circuit to vary the loading of the output cavity. With the output cavity coupling adjusted for maximum power output, the following test results were obtained:

E_b = 12 kV

I_b = 0.64 amp.

Power out = 3790 watts peak

Efficiency = 49.1%

Body current, average = 8 mA

Body current, peak = 60 mA

Duty factor = 0.1

During the course of testing it was discovered that by placing small pieces of iron within the magnetic circuit, the body current could be made to decrease. Access to the inside of the magnetic circuit was limited and placing the iron perturbers in the optimum position was difficult. Two iron discs approximately one-half inch in diameter and one-sixteenth inch thick were placed near the output cavity with the following results:

E_b = 12 kV

I_b = 0.64 amp.

Power output = 3800 watts peak

Efficiency = 49.5 %

Body current, average = 6.5 mA

Body current, peak = 32 mA

Duty factor = 0.1

51

Under these same conditions, the tube was then operated saturated cw:

$$E_b = 12 \text{ kV}$$
$$I_b = 0.64 \text{ amp.}$$
$$\text{Power output} = 3400 \text{ watts}$$
$$\text{Efficiency} = 44\%$$
$$\text{Body current} = 16 \text{ mA}$$

As seen, the power output had decreased due to thermal detuning of the output cavity. This also caused the bandpass to tilt downward toward the high-frequency edge.

The tube was next operated cw, at a beam voltage of 12 kV, with dc body current of 3.5 mA. The rf drive power was increased until the body current increased to 3.7 mA. The measured power output was 1510 watts and the body dissipation was measured calorimetrically at 56.5 watts. Since the body current had increased only a small amount, it was assumed that nearly all of the power dissipated in the body was due to output cavity circuit losses. This calculated to a circuit efficiency of 96.5%.

During cw operation at 3400 watts an arc occurred, in the output waveguide, causing the output window to fracture. The tube was rebuilt with a new output window and gun assembly. A load transformer, consisting of an inductive post brazed into the vacuum side of the output waveguide, was incorporated to reduce the external Q to 165.

At test, several small iron perturbers were again used to reduce the body current to a reasonable level. Final test results for this tube are summarized in Table 6.2.

Figure 6-5 shows the saturated bandpass at rf duty factors of 0.10 and 0.47. The displacement of the curve toward the low-frequency end at 0.47 duty is due to the thermal detuning of the output cavity.

Oscilloscope photographs of the bandpass characteristics for various rf drive levels at duties of 0.10 and 0.47 are shown in Figure 6-5A. The uppermost trace in each photograph represents saturated power output.
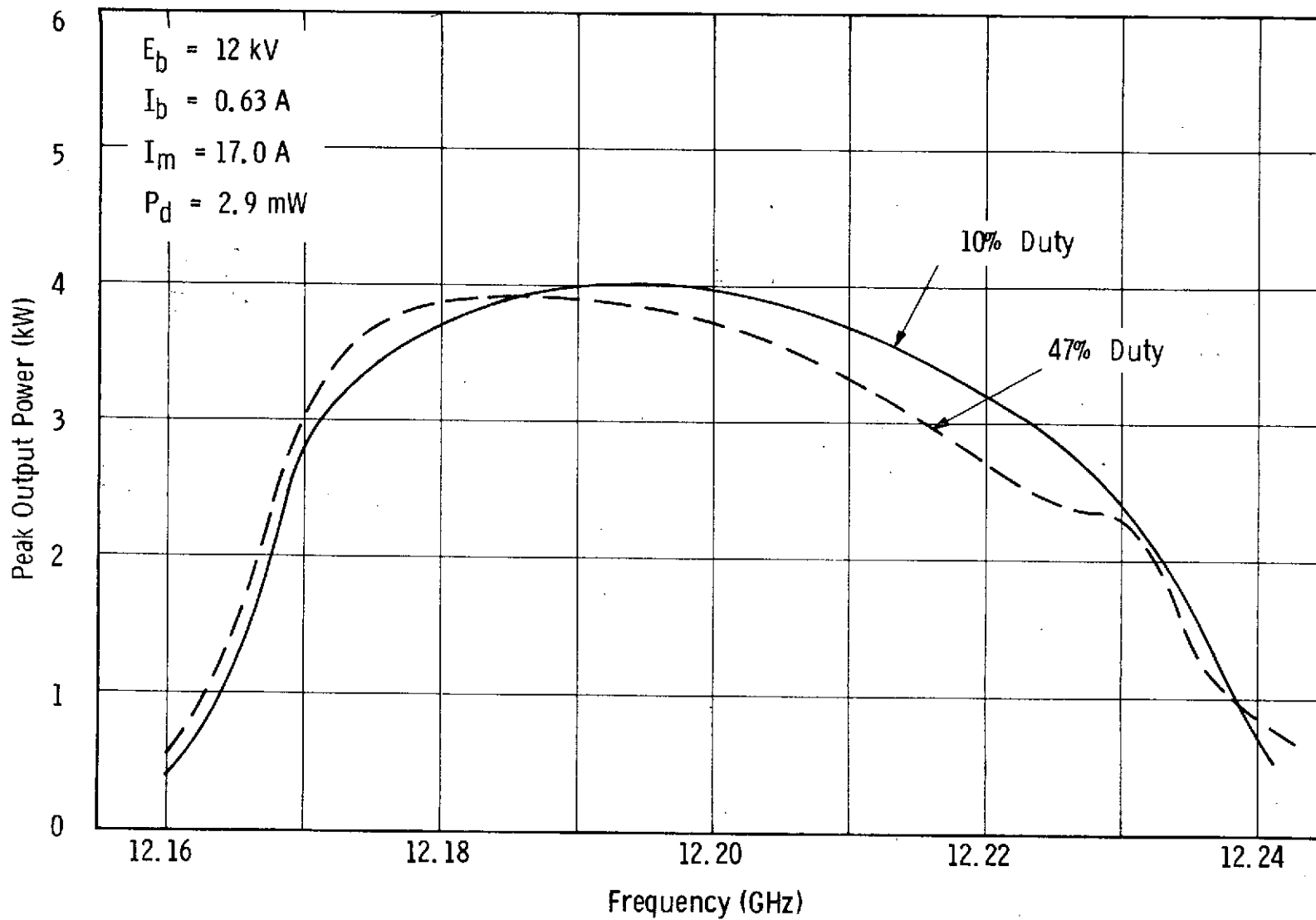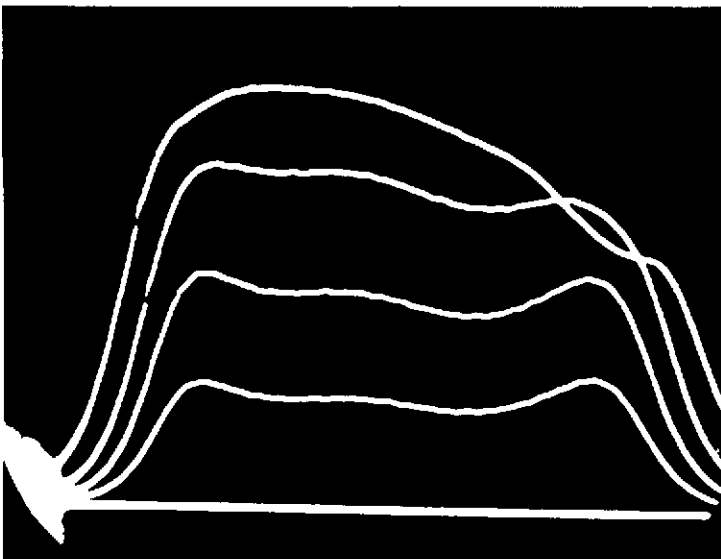
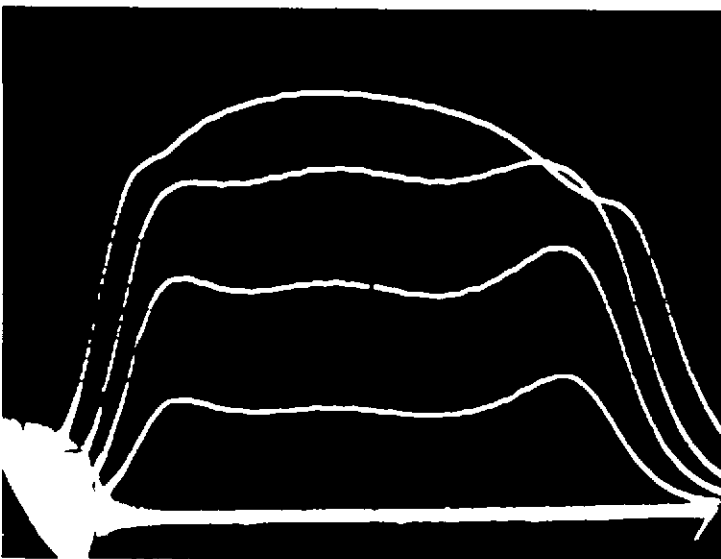Figure 6-5.   Peak Power Output vs Frequency VKX-7789 S. N. 1 R3

TP A-9221
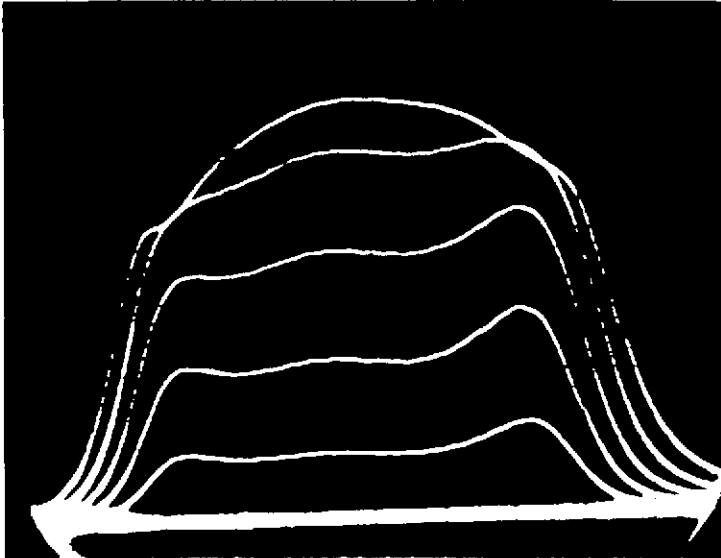
VKX-7789

No.1R3

10 kV

10% Duty

12.265 kV

47% Duty

12.265 kV

10% Duty

Figure 6-5A. Oscilloscope Photos of Bandpass Characteristics for Rf
Various Drive Levels

TABLE 6.2

FINAL TEST RESULTS ON SERIAL NUMBER 1 R3

Duty Factor	0.47	0.10	cw	—
Beam Voltage	12.0	12.0	10.0	kV
Beam Current	0.63	0.63	0.48	amp
Power Output, Peak	3900	4050	2020	W
Body Current, Average/Peak	10/15	*/20	2.3	mA
Body Current Without Rf	3	3	1.5	mA
Efficiency	51.5	53.5	42	%
Rf Input	2.9	2.9	*	mW
Solenoid Current No. 1	16	16	16	amp
Solenoid Current No. 2	17	17	16	amp
Bandwidth — 1 dB	43	47	45	MHz
Output Circuit Efficiency	95.5	95.5	95.5	%
Total Body Dissipation	159	*	126	W
Heater Voltage	9.0	9.0	9.0	Volts
Heater Current	2.55	2.55	2.55	amp

*Not measured

Using a quartz thermometer to obtain more accurate readings of body dissipation, the output circuit efficiency was again calculated. The final value was determined to be 95.5% instead of the previously measured 96.5%.

Because of the continuing thermal detuning problems with this tube, it was determined that the toroidal output cavity configuration used did not provide sufficient heat dissipation for satisfactory operating stability.

This was verified analytically, using the technique discussed in the final report for NASA Contract NAS3-11533 (Ref.3), for the determination of the temperature rise in a conical drift tube tip.

$$\Delta T = \int_{o}^{\ell} \frac{W_o\left(1 + \frac{W_1 x}{W_o \ell}\right)}{\pi\sigma_o\left[\left(r_1 + x\tan\theta\right)^2 - r_o^2\right]} \, dx$$

where:

x = distance measured from the tunnel tip

ℓ = length of conical section

θ = cone angle

W_o = beam power incident on the tunnel tip

W_1 = thermal power generated in the tunnel by rf losses and by beam incidence

σ_o = thermal conductivity of copper

r_o = tunnel inner radius

r_1 = outer radius at the tunnel tip

By assuming a constant drift tube angle of 20° and substituting the actual drift tube dimensions, this reduces to the approximation:

$$\Delta T = 2.8 \, W_o + 0.9 \, W_1$$

The worst case, in which all of the dc beam interception occurs in the output cavity, would then be given by:

$$W_o = I_{by} \text{ (dc)} \times E_b$$
$$= 0.003 \, (12000) = 36 \text{ watts}$$
$$= 18 \text{ watts/tip (approximate)}$$

and

$$W_1 = \frac{P_o}{\eta_{ckt}} - P_o$$

$$= \frac{2000}{.955} - 2000 = 94 \text{ watts}$$

$$= 31 \text{ watts/tip}$$

So that, for the test conditions of S/N 1R3:

$$\Delta T = 2.8(18) + 0.9(31) = 78°C$$

The expansion rate of copper is 0.018 mils/inch/°C, so that:

$$\Delta \ell = (0.018)(78)(0.103) = 0.145 \text{ mils/tip}$$

The measured gap-tuning rate for the toroidal cavity is 85 MHz/mil, and the total cavity frequency shift due to thermal detuning becomes:

$$\Delta f_o = 2(0.145)(85) = 25 \text{ MHz}$$

For cw operation at the 4 kW level, the calculated thermal detuning would become about 35 MHz.

Again, these are worst case numbers and the actual detuning due to drift tube growth would probably be somewhat less. The situation was undoubtedly aggravated by the poor cooling of the drift tube between penultimate and output cavity. It was decided at this point to increase the spacing between these two cavities to allow room for a water cooling passage around the drift tube. At the same time, the toroidal output cavity design was abandoned in favor of a more typical drilled cavity, allowing the use of heavier drift tubes with broader tip angle for improved thermal conduction. These changes were made on the second tube.

6.3 Serial Number 2 Test Results

The significant design modification made on the second tube was the change from the toroidal output cavity used on the first tube to a cavity of more common configuration. The initial approach was to use a cavity shape similar to the milled driver cavities. The drift tube shape selected was one with a 45° end taper, identical to the penultimate cavity, for good heat conduction.

A cold-test cavity was constructed for determination of the proper dimensions at the desired resonant frequency. The measured R/Q for the cavity was only 90. Assuming a Q_O of 2700, this gave a calculated output cavity circuit efficiency of 92.2%, which was considered inadequate for this tube design.

A new output cavity was then designed with 30° drift-tube tapers. This improved the measured R/Q to 120 and resulted in a calculated circuit efficiency of 94.2%. Calculations indicated that the thermal margin was still adequate. The Q_e of the output cavity for the second tube was adjusted to a value of 130, slightly overcoupled from the optimum value calculated 148, for improved stability and reduced output-cavity power dissipation. The final output-cavity configuration can be seen in the rf body layout drawing, Figure 6-6.

The drift length between the penultimate and output cavity gaps was increased slightly, from 0.254 inch on the first tube to 0.295 inch. This gave a normalized drift length of 35° and allowed a heavier copper web thickness for improved thermal conductivity and the addition of a water cooling passage.

The changes in the entrance and exit magnetic conditions derived on the first tube were also incorporated on the second. A measurement was made of the leakage magnetic field in the collector using the new output polepiece configuration, since it could not be done on the fully brazed body of the first tube. The results plotted in Figure 6-7 show that the specification, 0.5% of the main focusing field at a distance of two entrance hole diameters measured from the plane of the shield, is very nearly met even with the larger magnetic aperture.
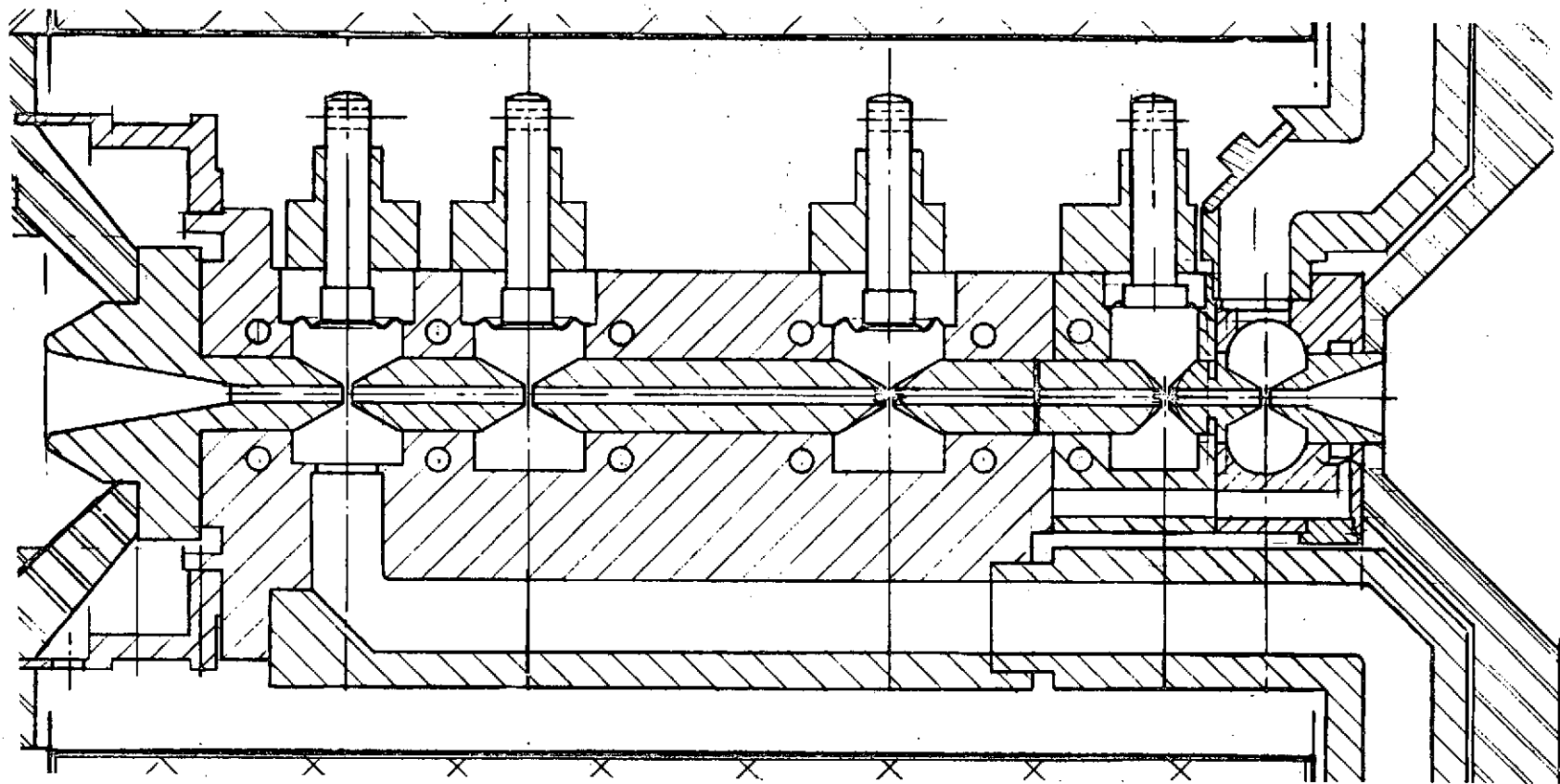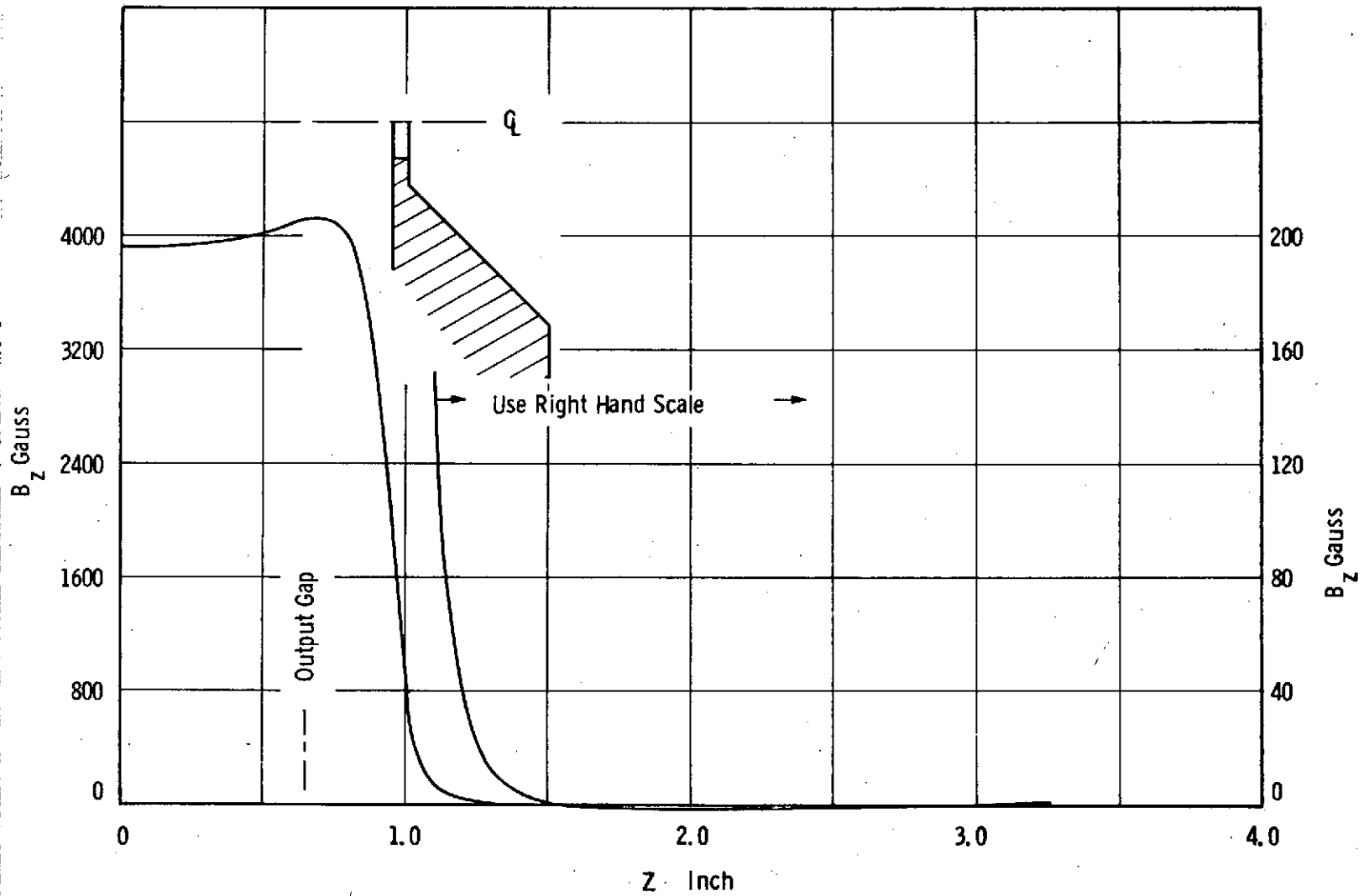
Figure 6-6. Final Rf Body Layout

Figure 6-7. Leakage Magnetic Field in Collector with Final Output
Polepiece Configuration

The gun package was modified to include external adjusting screws to allow optimization of beam performance. During early testing, while adjusting the alignment of the gun for best transmission, the brazed seal on the gun ceramic developed a vacuum leak. This was classified as an unfortunate occurrence, but not one that required a design change.

After the gun was repaired, the tube was again placed on test and the gun position adjusted, this time with no ill effect. Rf test results were similar to the first tube, but with greatly improved thermal stability. There was no evidence of output cavity detuning when going from low duty to cw operation. Final cw performance data are given in Table 6.3.

TABLE 6.3

FINAL TEST RESULTS ON SERIAL NUMBER 2

Frequency	12.184 MHz
Beam Voltage	12.3 kV
Beam Current	0.659 amp
Power Output	4.0 kW
Body Current, rf	13 mA
Body Current, dc	4 mA
Efficiency	49.3%
Rf Drive Power	1.3 mW
Bandwidth, 1 dB	47 MHz
Heater Voltage	9.0 volts
Heater Current	2.4 amps
Solenoid Current	19.6 amps

The measured output-cavity circuit efficiency was 95.4%, which compares favorably with the final value measured on the first tube with the toroidal output cavity.

Figure 6-8 shows the tube bandpass as a function of rf drive level.

Figure 6-9 illustrates the saturated bandpass at normal and reduced beam voltages.

This tube came very close to meeting all of the specification goals set forth in the contract, and no design changes were warranted for the third and final tube.
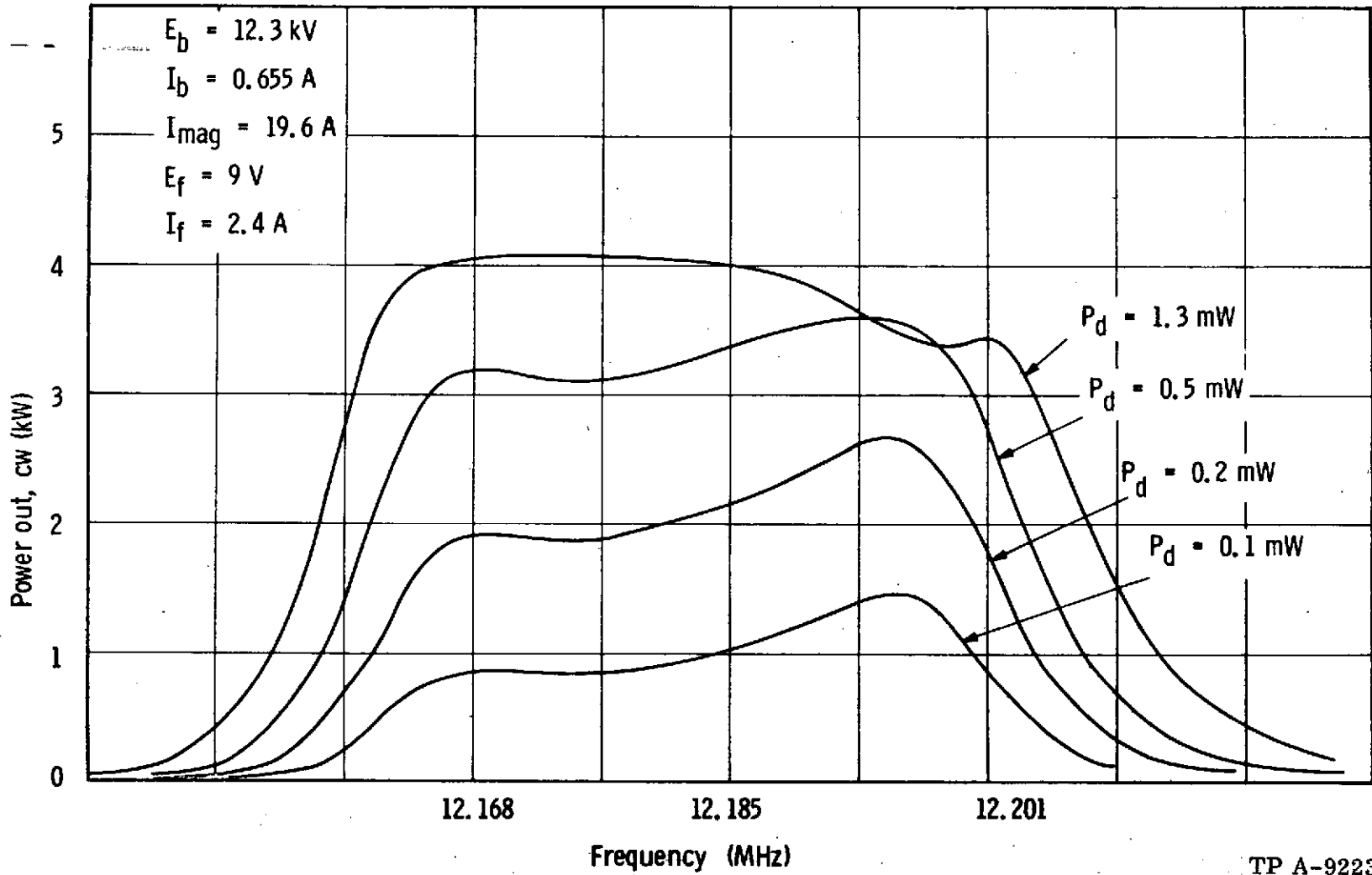
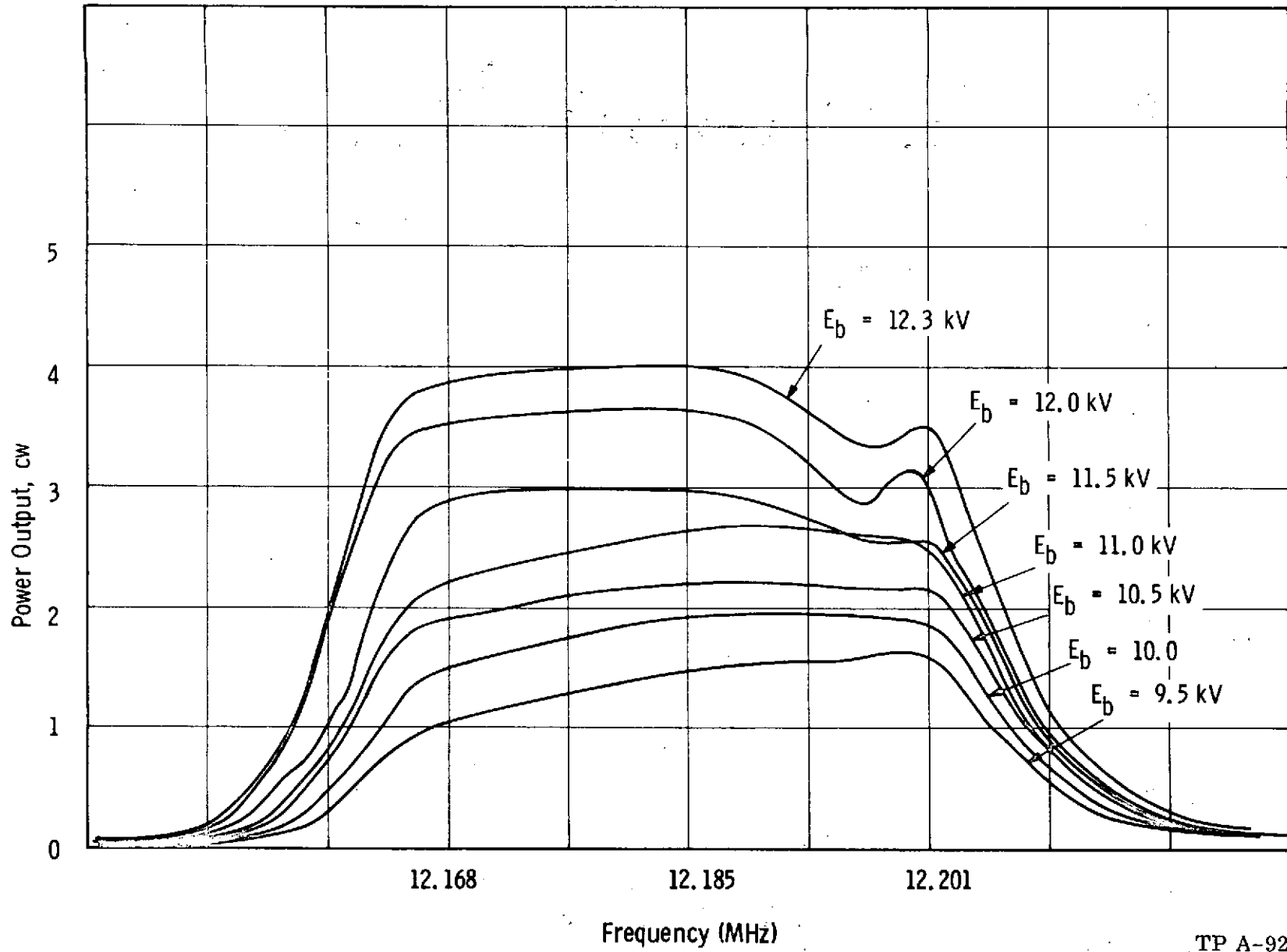Figure 6-8. Tube Bandpass as a Function of Rf Drive Level VKX-7789 S. N. 2

Figure 6-9.   Saturated Bandpass at Normal and Reduced Beam Voltages
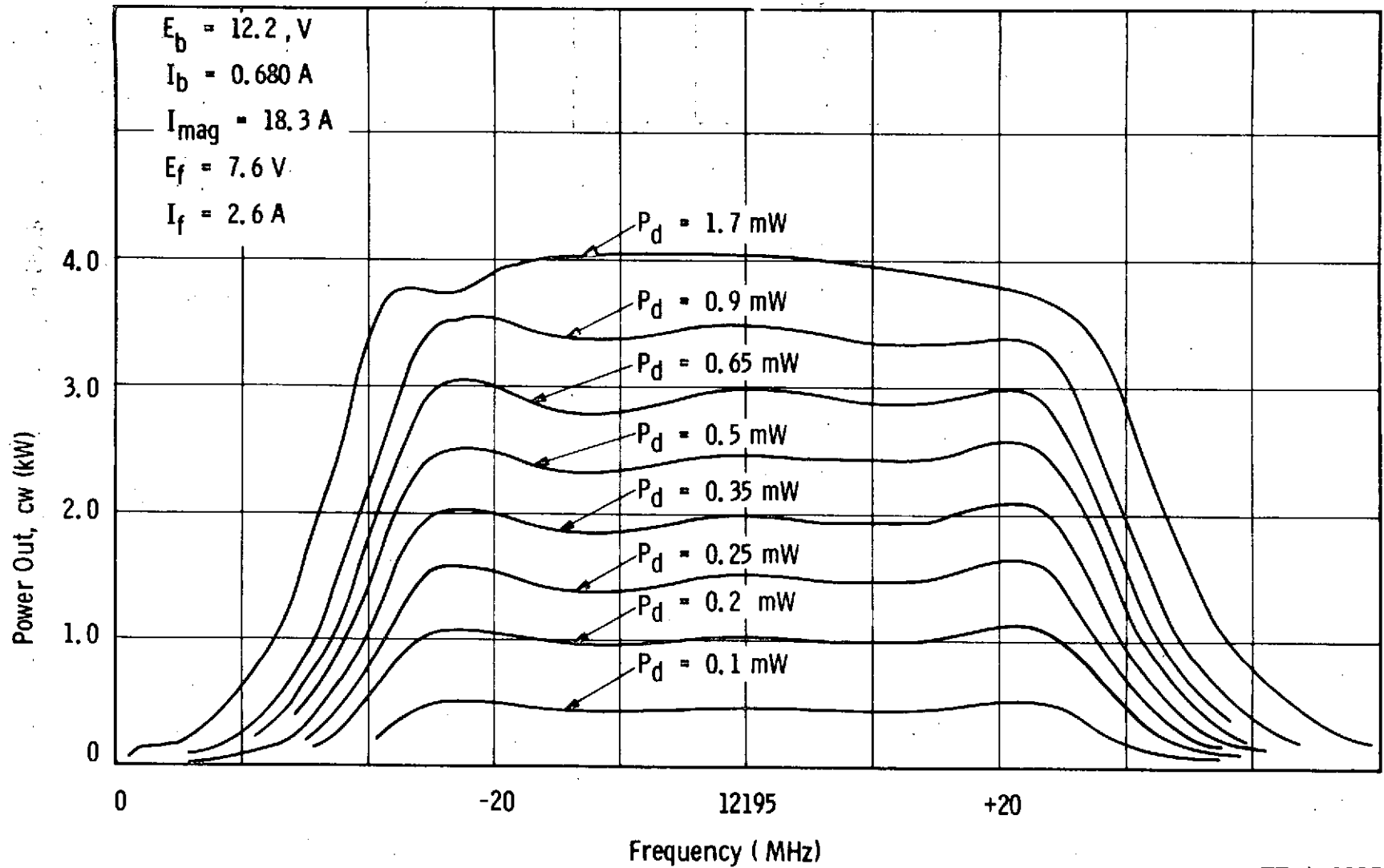VKX-7789 S. N. 2

TP A-9224

6.4 Serial Number 3 Test Results

Within reasonable manufacturing variation, the third tube was identical in all respects to the second. No undue problems were experienced in either fabrication or test. The results of rf testing are tabulated in Table 6.4.

TABLE 6.4

FINAL TEST RESULTS ON SERIAL NUMBER 3

Frequency	12.195	12.195	12.195	12.195	GHz
Beam Voltage	12.2	11.5	11.0	10.0	kV
Beam Current	0.685	0.630	0.590	0.515	amp
Power Output	4070	3240	2815	2120	watts
Body Current, rf	18.5	15.0	14.0	7.0	mA
Body Current, dc	1.5	1.5	1.5	1.5	mA
Efficiency	48.4	44.7	44.5	40.7	%
Rf Drive Power	2.0	2.6	3.7	3.3	mW
Bandwidth, 1 dB	>40	>40	>40	>40	MHz
Heater Voltage	7.6	7.6	7.6	7.6	volts
Heater Current	2.6	2.6	2.6	2.6	amps
Solenoid Current	18.35	18.35	18.1	18.2	amps

The gain flatness across the operating frequency band was somewhat better than for the second tube, although the center frequency was approximately 5 MHz lower than the design center, due to a slight mistuning of the output cavity. The bandpass response for several rf drive levels is shown in Figure 6-10. Gain linearity at the 12.195 GHz center frequency is plotted in Figure 6-11.

Figure 6-10. Cw Power Output vs Frequency with Drive Level as a Parameter VKX-7789 S. N. 3

TP A-9225

65
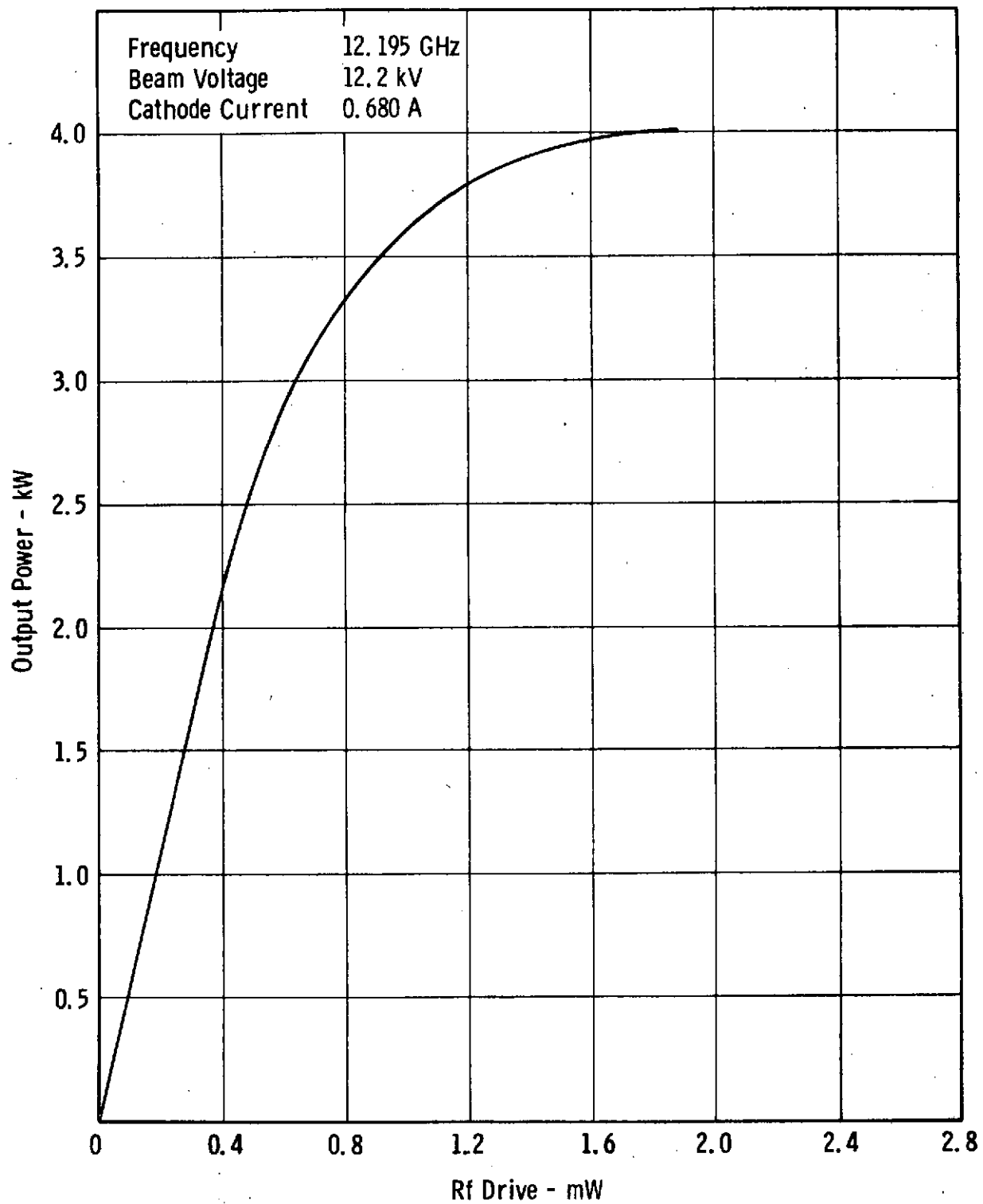
Figure 6-11.   Gain Linearity at 12. 195 GHz Center Frequency VKX-7789 S. N. 3

7.0 CONCLUSIONS

An experimental program has been undertaken to demonstrate the feasibility of techniques for achieving high conversion efficiency in a 4 kW cw klystron amplifier at 12.2 GHz.

The design of the tubes constructed on this program was based on an approach for increasing the conversion efficiency through utilization of the second harmonic space-charge forces in the bunched beam. Computational analysis has indicated that this design technique can result in efficiencies of greater than 60%.

The first tube built employed a toroidal output cavity, since analysis had shown that the internal Q factor could be maximized by using this configuration. This is essential in achieving lower internal power dissipation and hence higher circuit efficiency. For this tube the measured output cavity internal Q was 3100, and the measured circuit efficiency was 95.5%, both values slightly higher than those calculated from theory. The R/Q was measured to be 85. The maximum measured conversion efficiency was 53.5%.

The sacrifice paid for this performance was a high degree of thermal frequency drift in the output cavity. This was traced to the dimensional change in the drift tube tips, resulting from the temperature rise due to intercepted beam power and rf cavity losses, and aggravated by inadequate cooling of the drift tube section between the penultimate and output cavities. For highest efficiency, the computed optimum drift length between these two cavities is physically so short at this operating frequency that space is not available for either an effective coolant channel or material thickness adequate for good thermal conductive cooling.

Due to the thermal detuning problems experienced on the first tube, the design of the second tube was modified to increase the penultimate drift length to allow the addition of a coolant passage in that region. At the same time, the toroidal output cavity design was abandoned in favor of a more conventional rectangular design with heavier-walled cylindrical drift tubes to provide a reduced temperature rise. In retrospect, this second step may not have been necessary, since the

relative ΔT computed for each case was not sufficiently different to account for the improvement seen on the second tube.

The measured internal Q for the new output cavity design was approximately 2500, but the R/Q had increased to 120. At test, the effects of thermal detuning had decreased to a very acceptable level. With full cw output power, the conversion efficiency was 49%, slightly below that of the first tube, due to the nonoptimum penultimate drift length. However, the measured output cavity circuit efficiency was 95.4%, approximately the same as before.

A third tube was constructed with the same design as the second, and performance results were essentially the same.

The experimental results on these tubes, therefore, substantiate the improvement in internal Q offered by a cavity of toroidal configuration. However, the lower R/Q achievable with such a cavity to some degree offsets this improvement, and results in an overall output circuit efficiency that is approximately the same as that seen with a more conventional rectangular cavity.

Comparative measurements in the two cases cited were compromised to some extent by the differences in cavity and drift tube cooling, which could probably account for the toroidal cavity running at a somewhat higher temperature with correspondingly higher resistivity of the copper surface. To eliminate the effects of this uncertainty, a tube would have to be constructed with a toroidal output cavity, but with the improved cooling design used on the second and third tube.

The program has also shown that a goal of 50% conversion efficiency for a 4 kW klystron at 12.2 GHz is an achievable reality, and that thermal considerations are an extremely important part of the physical design at the higher microwave frequencies.

Varian Associates
Palo Alto Tube Division
Palo Alto, California
December 14, 1973

8.0 REFERENCES

1. Kavanagh, Francis E.; Alexovich, Robert E.; and Chomos, Gerald J.: Evaluation of Novel Depressed Collector for Linear-Beam Microwave Tubes. NASA TM X-2322, 1971.

2. Kosmahl, Henry G.: A Novel, Axisymmetric, Electrostatic Collector for Linear Beam Microwave tubes. NASA TN D-6093, 1971.

3. Branch, G. M.: Circuit Efficiency Enhancement Studies at 12 GHz. Final Report, NASA Contract NAS3-11533, 1970.

4. Lien, Erling L.: High Efficiency Klystron Amplifiers. Eighth International Conference on Microwave and Optical Generation and Amplification, Amsterdam, Sept 1970, Section II, pp. 21-27.

5. Branch, G. M.; Mihran, T. G.: Analytical Designs of a Space-Borne Magnetically-Focused Klystron Amplifier. NASA CR-72461, 1968.

6. Lien, E. L.: Large-Signal Analysis of Klystrons. International Electron Devices Meeting, Washington, DC, October 1968.

7. Pierce, J. R.: Theory and Design of Electron Beams. D. Van Nostrand Co., Inc., 1954.

APPENDIX A

LIST OF SYMBOLS

a	drift tube inner radius
b	beam radius
c	free-space velocity of light
E_b	dc beam voltage
E_f	heater voltage
I_b	dc beam current
I_{by}	body current
I_f	heater current
Imag	focusing solenoid current
ℓ	axial length
M	cavity gap coupling coefficient
P_d	rf drive power
P_o	output power
Q	quality factor of resonant cavity
Q_o	unloaded Q
Q_e	external Q
Q_L	total loaded Q
R, R_{sh}	cavity interaction gap shunt resistance
u_o	dc beam velocity
V_o	dc beam voltage
VSWR	voltage standing wave ratio
β_e	propagation factor associated with the dc beam velocity $(\beta_e = \omega/u_o)$
β_q	plasma propagation factor $(\beta_q = \omega q/u_o)$
γ	relativistic propagation factor $\left(\gamma = \beta_e \left[1 - (u_o/c)^2\right]^{1/2}\right)$
η	conversion efficiency
ϕ	rf phase shift
ω	angular frequency
ωq	reduced plasma angular frequency